S. Soldini, C. Colombo, S.J. I. Walker
Solar Radiation Pressure Hamiltonian Feedback Control for Unstable Libration-Point Orbits
Journal of Guidance Control and Dynamics, Vol. 40, N. 6, 2017, p. 1374-1389
doi:10.2514/1.G002090

JOURNAL OF GUIDANCE, CONTROL, AND DYNAMICS
Vol. , No. ,

Solar Radiation Pressure Hamiltonian Feedback Control for Unstable Libration-Point Orbits

Stefania Soldini,* Camilla Colombo,† and Scott J. I. Walker‡
University of Southampton, Southampton, England SO17 1BJ, United Kingdom

DOI: 10.2514/1.G002090

This work investigates a Hamiltonian structure-preserving control that uses the acceleration of solar radiation pressure for the stabilization of unstable periodic orbits in the circular restricted three-body problem. This control aims to stabilize the libration-point orbits in the sense of Lyapunov by achieving simple stability. It also preserves the Hamiltonian nature of the controlled system. The Hamiltonian structure-preserving control is then extended to a general case in which complex and conjugate eigenvalues occur at high-amplitude orbits. High-amplitude orbits are currently of interest to the European Space Agency for future libration-point orbit missions because they require a lower insertion Δv compared to low-amplitude orbits. Based on the design of the feedback control, the purpose of this work is to verify when the use of solar radiation pressure is feasible and to determine the structural requirements and the spacecraft's pointing accuracy.

Nomenclature

A	=	area, m^2
a_x^s	=	x component of solar radiation pressure acceleration
a_y^s	=	y component of solar radiation pressure acceleration
a_z^s	=	z component of solar radiation pressure acceleration
$\boldsymbol{a}^c$	=	Hamiltonian structure-preserving control acceleration
$\boldsymbol{a}^s$	=	solar radiation pressure acceleration
Df	=	matrix of the linearized dynamics
Df^c	=	matrix of the controlled linearized dynamics
$G_{1,2,3}$	=	control gains of the Hamiltonian structure-preserving control law
I	=	identity matrix
$L_{1,2}$	=	libration points 1 and 2
M	=	monodromy matrix
$\hat{\boldsymbol{N}}$	=	unitary vector normal to the reflective area
$\boldsymbol{r}$	=	spacecraft vector position in the rotating system
$\boldsymbol{r}_{\text{Earth}-p}$	=	spacecraft–Earth distance in the rotating system
$\boldsymbol{r}_{\text{Sun}-p}$	=	spacecraft–sun distance in the rotating system
$\dot{\boldsymbol{r}}$	=	spacecraft vector velocity in the rotating system
T	=	Hamiltonian structure-preserving control matrix
T	=	orbital period
t	=	actual integration time
t_0	=	initial time
$\boldsymbol{u}_k$	=	normalized control eigenvectors
$\boldsymbol{u}_k \cdot \boldsymbol{u}_k^T$	=	projection tensor
V	=	total potential
V_{rr}	=	double derivatives of the total potential
V_x	=	x component of total potential
V_y	=	y component of total potential
V_z	=	z component of total potential
V_{rr}^c	=	double derivatives of the controlled total potential
$\boldsymbol{X}$	=	spacecraft state vector in the rotating system
x	=	x component of the spacecraft position in the rotating system
$\hat{\boldsymbol{x}}_k$	=	eigenvectors of the linearized equations of motion
$\dot{x}$	=	x component of the spacecraft velocity in the rotating system
y	=	y component of the spacecraft position in the rotating system
$\dot{y}$	=	y component of the spacecraft velocity in the rotating system
z	=	z component of the spacecraft position in the rotating system
$\dot{z}$	=	z component of the spacecraft velocity in the rotating system
α	=	reflective area's in-plane angle, deg
β	=	lightness parameter
Δv	=	variation in the spacecraft velocity
δ	=	reflective area's out-of-plane angle, deg
$\delta\boldsymbol{r}$	=	position error between the actual spacecraft position and the target orbit
$\delta\dot{\boldsymbol{r}}$	=	velocity error between the actual spacecraft position and the target orbit
λ_k	=	eigenvalues of the linearized equations of motion
μ	=	mass parameter of the system
μ_{Earth}	=	mass parameter of the Earth
μ_{Sun}	=	mass parameter of the sun
Φ	=	state transition matrix
Φ	=	spacecraft–sun vector's in-plane angle, deg
Ψ	=	spacecraft–sun vector's out-of-plane angle, deg

Received 4 May 2016; revision received 11 November 2016; accepted for publication 15 December 2016; published online XX epubMonth XXXX.

*Ph.D. Candidate, FEE/Astronautics Research Group; s.soldini@soton.ac.uk.
†Lecturer, FEE/Astronautics Research Group; c.colombo@soton.ac.uk.
‡Associate Professor, FEE/Astronautics Research Group; sjiw@soton.ac.uk.

I. Introduction

IN CELESTIAL mechanics, the motion of a spacecraft under the mutual gravitational influence of the sun and the Earth + moon is known as the restricted three-body problem. In this problem, five equilibrium solutions of the equations of motion can be found. These equilibrium points, known as libration points, are defined with respect to the coordinate system rotating with the sun–(Earth + moon) [1,2]. Currently, the libration points selected for space applications are the collinear points that are aligned with the sun–(Earth + moon). In particular, L_1 is located between the sun and the Earth + moon and L_2, where the Earth is located between the sun and L_2. Spacecraft are usually placed in libration-point orbits (LPOs) that are in the vicinity of the equilibrium points $L_{1,2}$ rather than at the equilibrium points because of the large Δv required to position a spacecraft at $L_{1,2}$. Moreover, the Earth–spacecraft communication link is complicated by the sun–Earth and L_1 alignment. Libration-point orbits are periodic or quasi-periodic orbits that are relatively inexpensive to reach via a direct launch from Earth. Orbits around L_1 are usually preferred platforms when studying the sun, whereas orbits near L_2 are selected for deep-space observations [3].

In 1968, Farquhar proposed to exploit LPOs around the Lagrangian points of the Earth–moon system as a communication

relay on the far side of the moon [4]. The interest of the space agencies in LPOs started after the success of the ISEE-3 mission. There are numerous examples of LPO missions founded by the various space agencies. SOHO currently studies the sun's outer corona [5], and the Herschel mission was designed to investigate the formation of galaxies [6]. The European Space Agency (ESA) succeeded in launching the Gaia space telescope in 2013 [7], whereas NASA/ESA/CSA's James Webb Space Telescope will provide astronomical measurements to understand the formation of our universe. A concurrent mission by ESA, called Euclid, will map the geometry of the dark universe [8].

Distant prograde orbits (DPOs) are, instead, planar periodic orbits around the Earth in the sun–Earth system, which are also known as family g [9]. DPOs are unstable but can be exploited to perform orbital transfer within the sun–Earth system. They have been used by various missions, such as NASA's Wind mission, to transfer between LPOs around L_1 and L_2, showing that transfer composed by DPO arcs requires a low transfer Δv [10]. Lara and Russell [11] suggested the use of distant orbits around the smaller body for studying the planetary satellites of a general system: for example, to study an asteroid in a sun–asteroid system [12] or moons in a planet–moon system. The advantage of distant orbits is the possibility to make observations of the smaller body without interacting with its highly perturbed environment. Note that, although DPOs can be either stable or unstable for the sun–(Earth + moon) system, they are always unstable in the case of Deimos (i.e., the Mars–Deimos system) [13]. This evidences the importance of performing station keeping for spacecraft in DPOs for a general mission scenario.

However, a spacecraft placed at LPOs and DPOs will naturally move away from the nominal trajectory because of small perturbations. Such natural perturbations cause instabilities to LPOs and DPOs; therefore, yearly station-keeping maneuvers are required to counteract their effects [14]. This paper investigates a Hamiltonian structure-preserving (HSP) propellant-free control that exploits the natural perturbed environment of the restricted three-body problem. When looking at the sun–Earth system, one of the major perturbations after the gravitational effects is the solar radiation pressure (SRP). A recent idea was to design control strategies based on the exploitation of SRP to allow a significant reduction in the amount of the required onboard propellant. The SRP acceleration magnitude is a function of the spacecraft's area-to-mass ratio, the spacecraft's orientation angles, and the material reflectivity properties. Thus, reflective deployable structures can potentially control the spacecraft through SRP acceleration to perform station keeping. Indeed, the first concept of SRP stabilization was proposed for attitude control in 1959 [15], and geosynchronous satellites such as OTS, TELECOM 1, and INMARSAT 2 have successfully implemented control strategies based on SRP. For attitude control, an asymmetrical offset of solar array wings from the nominal sun-pointing orientation can be maintained to generate the "windmill" torques [15].

In the framework of control theory for LPOs, the existing control strategies are distinguished between linear and nonlinear controllers, where some of them have also been extended to SRP applications. Among the nonlinear controls, Xin et al. [16] developed a suboptimal control known as the θ-D technique, which established the control stability by using Lyapunov theory. Shahid and Kumar [17] proposed a sliding-mode control for formation flight, enhanced by SRP, where both the orientation angle and the area were control parameters. Gómez et al. [18,19] used the invariant manifold theory by exploiting the Floquet modes to design the control law. Howell and Pernicka [20] developed the target point technique where, as for the FM approach, ΔV is computed to keep the spacecraft near the nominal trajectory. Both the techniques were compared by Keeter [21] and then extended to SRP applications by McInnes [22] for the target point method and by Farrés and Jorba [23–24], CeriottaandFarrés [25], and Farrés and Jorba[26] for the Floquet mode method. In both cases, the only control parameter was the sail orientation angle, whereas the area was kept constant. Scheeres et al. [27] proposed a HSP control that stabilized the system in the sense of Lyapunov and applied it with low-thrust propulsion in formation-flight applications. Scheeres et al.'s control law was then extended by Xu and Xu [28] for SRP applications where both the area and the in-plane orientation angle were included as control parameters. Finally, the linear quadratic regulator technique in solar sail applications was first developed by Bookless and McInnes [29] and then by Ceriotti and Farrés [25] where, in both cases, the sail's area and orientation angles were the control parameters.

In this paper, the aim is to exploit the invariant manifold theory to select and design a control law compatible with SRP propulsion for spacecraft in high-amplitude DPOs. Thus, the HSP is then selected as a candidate for SRP propulsion because it has been shown to work with nonlinearities. The HSP control law proposed by Scheeres et al. [27] works in the case of low-amplitudes orbits, whereas it fails to control spacecraft placed in high-amplitude DPOs. This behavior is due to the fact that, when studying the Lyapunov stability, the further the spacecraft is away from the equilibrium point, the more the stability along the orbit changes. In this particular case, a HSP control law based on the work of Scheeres et al. [27] and Xu and Xu [28] is proposed, but it is extended to a general case, in which complex and conjugate eigenvalues (i.e., stable–unstable foci) occur. Note that the orbit's amplitude in the y axis A_y is the important parameter that determines the occurrence of complex and conjugate eigenvalue pairs.

Once the HSP control acceleration is generalized independently to the size of the periodic orbit's amplitude, it is then investigated if this required control acceleration can be achieved by actuators on board the spacecraft that control the effect of SRP. These actuators could control the reflectivity of the spacecraft, the reflective area illuminated by the sun, or by changing the spacecraft orientation. Finally, the HSP control law designed for high-amplitude DPOs is then tested for harnessing SRP.

This paper is organized as follows: Sec. II presents the equations of motion, whereas in Sec. III, the HSP control law is shown for low-amplitude orbits and is extended to high-amplitude orbits. Then, the conditions for the gains selection is demonstrated in Sec. IV. The SRP actuator model is shown in Sec. V, whereas a note on the Lyapunov stability is presented in Sec. VI. Finally, the HSP control is applied to SRP propulsion for LPOs (i.e, SOHO mission) and DPOs (i.e, family a and family g) missions, as shown in Sec. VII.

II. Dynamical Model

The spacecraft's dynamics is described by the circular restricted three-body problem under the influence of solar radiation pressure. The equations of motion are written with respect to the rotating frame in dimensionless coordinates and units:

$$\begin{cases} \ddot{x} - 2\omega_0 \dot{y} = V_x + a_x^s \\ \ddot{y} + 2\omega_0 \dot{x} = V_y + a_y^s \\ \ddot{z} = V_z + a_z^s \end{cases} \tag{1}$$

where x, y, z and $\dot{x}$, $\dot{y}$, $\dot{z}$ are, respectively, the spacecraft positions and velocities in the rotating frame. The spacecraft's mass is assumed to be infinitesimal with respect to the sun–(Earth + moon) masses. Both the sun and the Earth + moon are assumed to be point masses, and their motion is described by a circular orbit around their center of mass. In Eq. (1), V is the total potential:

$$V = \frac{1}{2}(x^2 + y^2) + \frac{\mu_{\text{Sun}}}{r_{\text{Sun}-p}} + \frac{\mu_{\text{Earth}}}{r_{\text{Earth}-p}} \tag{2}$$

which includes the potential effects of the rotating system (first term in the right-hand side) and the sun and the Earth + moon gravitation with normalized angular velocity ω_0, which is equal to one. When the effect of the sun radiation is included, the SRP acts as a repulsive force with respect to the sun's gravitational force [1,30]. In Eq. (1), a_x^s, a_y^s, and a_z^s represent the SRP acceleration components of $\boldsymbol{a}^s$, which is defined as follows [23]:

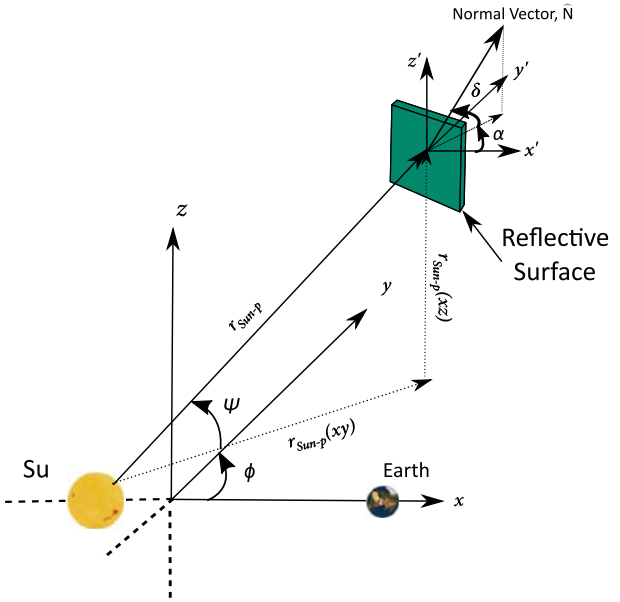

Fig. 1 Definitions of α, Ψ, δ, and Φ angles.

$$\boldsymbol{a}^s = \beta \frac{\mu_{\text{Sun}}}{r^2_{\text{Sun}-p}} \cdot \left\langle \frac{\boldsymbol{r}_{\text{Sun}-p}}{|\boldsymbol{r}_{\text{Sun}-p}|}, \hat{\boldsymbol{N}} \right\rangle^2 \cdot \hat{\boldsymbol{N}}$$
$$\hat{\boldsymbol{N}} = \begin{Bmatrix} \cos(\Phi+\alpha)\cdot\cos(\Psi+\delta) \\ \sin(\Phi+\alpha)\cdot\cos(\Psi+\delta) \\ \sin(\Psi+\delta) \end{Bmatrix} \tag{3}$$

where β is the lightness parameter that assumes values from zero (no SRP effect) to one (SRP force is equal to the sun gravitational force[§]). The lightness parameter, $\beta = \sigma^*/\sigma$, is a function of the mass-to-area ratio σ and the sun luminosity of $\sigma^* = 1.53$ g/m^2 [31].

The lightness parameter is a function of the reflectivity coefficient c_R and the area-to-mass ratio through the following:

$$\beta = P_{\text{srp}-1\text{AU}} \frac{r^2_{\text{Earth}-\text{Sun}}}{\mu_{\text{Sun}}} \frac{A}{m} c_R \tag{4}$$

where $P_{\text{srp}-1\text{AU}}$ is the solar pressure at 1 AU.

Figure 1 shows $\hat{\boldsymbol{N}}$, which is the normal to the reflective surface, where the angles Φ and Ψ describe the spacecraft–sun vector with respect to the rotating system $\{x, y, z\}$. Instead, α and δ are the angles between the spacecraft–sun vector and $\hat{\boldsymbol{N}}$ projected to the $x-y$ plane and $y-z$ plane, respectively, and they can assume values between $-\pi/2$ and $\pi/2$ [23,32].

In Eqs. (2–3), $r_{\text{Sun}-p}$ and $r_{\text{Earth}-p}$ are defined such that

$$r_{\text{Sun}-p} = \sqrt{(x - x_{\text{Sun}})^2 + y^2 + z^2}$$
$$r_{\text{Earth}-p} = \sqrt{(x - x_{\text{Earth}})^2 + y^2 + z^2} \tag{5}$$

where $x_{\text{Sun}} = -\mu$ is the position of the larger primary (i.e., sun) and $x_{\text{Earth}} = 1-\mu$ is the position of the smaller primary (i.e., Earth + moon); moreover, the dimensionless masses of the primaries are defined as $\mu_{\text{Earth}} = \mu$ and $\mu_{\text{Sun}} = 1-\mu$. For the sun–(Earth + moon) model, the value of μ, which is the mass parameter of the system, is in nondimensional units [33].

Equation (1) refers to the general case; however, for a planar case, only the first two equations in Eq. (1) hold and their dependence to the z components is cancelled. If the SRP is not included in the model, then the dependence to a^s_x, a^s_y, and a^s_z is cancelled too. Finally, there are special cases in which the SRP is included in the system, but its effect is zero and it occurs when $\boldsymbol{r}_{\text{Sun}-p}/|\boldsymbol{r}_{\text{Sun}-p}|$ and $\hat{\boldsymbol{N}}$ are perpendicular vectors: in other words, when α or δ are equal to $\pm\pi/2$.

[§]$\beta = 1$ is just a theoretical value; it is not achievable for real applications.

III. Design of Control Law that Preserves the Hamiltonian Structure of the System

The Hamiltonian structure-preserving control uses the eigenstructure of the linearized equations of motion, evaluated along the orbit, to design a control law that ensures Lyapunov stability [34]. As shown by Scheeres et al. [27], this controller aims to compensate the stable and unstable components of the system by projecting the state position error (between the current and the target orbit) along the eigenvectors direction. This creates an artificial center manifold that keeps the trajectory close to the target orbit, as the eigenvalues of the linearized dynamics are placed along the imaginary axis. Thus, the local stability (simple Lyapunov stability of the linearized equations of motion evaluated along the orbit) impacts onto the LPO stability (stability at each orbital period) by affecting the eigenvalues of the monodromy matrix M that is the state transitional matrix $\Phi(T, t_0)$ of the system evaluated after one orbital period T, where t_0 is the initial time. For Lyapunov stability, the controller should place the eigenvalues of M on the unitary circle of the complex plane [35]; see Fig. 2. Thanks to the effect of the control, matrix M is still symplectic because $M^T \boldsymbol{\Omega} M = \boldsymbol{\Omega}$ with

$$\boldsymbol{\Omega} = \begin{bmatrix} 0 & I \\ -I & 0 \end{bmatrix}$$

but the existence of a Jacobi integral is no longer guaranteed because the central two real solutions equal to one are removed. Moreover, the fact that the monodromy matrix is symplectic also guarantees that the system is still autonomous and Hamiltonian [27]. Note that the effect of the control does not preserve the Hamiltonian of the original dynamical system; however, after the effect of the control law, the controlled system has a new Hamiltonian structure. Scheeres demonstrated that the study of local stability is connected to the periodic orbit stability. This will be summarized in the following because it is useful to introduce the extension of the controller proposed in this work. At first, the equations of motion are linearized around the equilibrium point. The variational equations of Eq. (1) are [30]

$$\frac{\mathrm{d}}{\mathrm{d}t}\begin{bmatrix} \delta\boldsymbol{r} \\ \delta\dot{\boldsymbol{r}} \end{bmatrix} = \begin{bmatrix} \boldsymbol{0} & I \\ V_{rr} & 2\omega_0 \boldsymbol{J} \end{bmatrix}\begin{bmatrix} \delta\boldsymbol{r} \\ \delta\dot{\boldsymbol{r}} \end{bmatrix}, \quad \text{where } \boldsymbol{J} = \begin{bmatrix} 0 & 1 \\ -1 & 0 \end{bmatrix} \tag{6}$$

V_{rr} is the Hessian matrix of the potential acceleration in Eq. (2), and $2\omega_0 \boldsymbol{J}$ is the term associated to the Coriolis acceleration. In Eq. (6), $\delta\boldsymbol{r}$ and $\delta\dot{\boldsymbol{r}}$ are the state position and velocity errors, respectively. The eigenvalues of the linearized dynamics evaluated along the LPO are the solutions of the characteristic equation $D(\lambda) = |Df - \lambda I| = 0$, where the characteristic polynomial is

$$\Lambda^2 + b\Lambda + c = 0 \quad \text{where} \begin{cases} b = 4\omega_0^2 - V_{xx} - V_{yy} \\ c = V_{xx}V_{yy} - V^2_{xy} \\ \Delta = b^2 - 4c \end{cases} \tag{7}$$

As exploited by Scheeres, the solutions of Eq. (7) are affected by the sign of Δ. When $\Delta > 0$, the system admits two real and unequal roots, whereas when $\Delta < 0$, there are two complex and conjugate

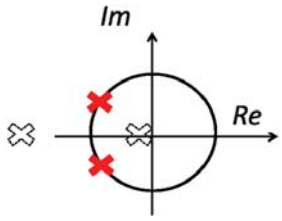

Fig. 2 Eigenvalues of the monodromy matrix with (filled crosses) and without (empty crosses) the effect of the HSP controller.

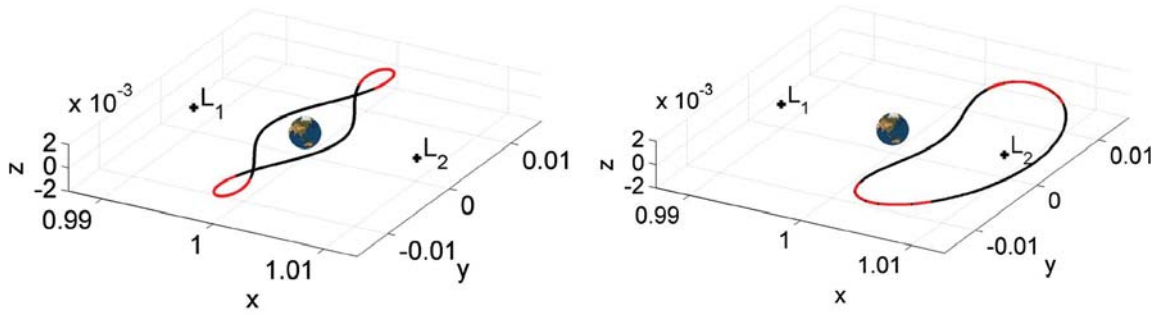

a) Distant prograde orbit b) Planar-lyapunov

Fig. 3 Eigenvalues along the LPO, showing the hyberbolic × center solutions (inner arcs) and the couples of complex and conjugate solutions (outer arcs). (Note that the Earth is not to scale.).

solutions. The change in the eigenvalues stability is evident for high-amplitude orbits where it is possible to identify two cases along the trajectory where the eigenvalues are couples of real and pure imaginary numbers (saddle × center equilibrium; i.e., the black lines in Figs. 3a and 3b, when $b < 0$, $\Delta > 0$, and $c < 0$) or where the eigenvalues are couples of complex numbers and conjugate pairs (stable × unstable foci; i.e., the lines in Figs. 3a and 3b, when $b < 0$, $\Delta < 0$, and $c < 0$). For example, in the case of family g, the appearance of foci happens above $A_y = 0.02$ dimensionless units. Above $A_y = 0.02$, family g shows the appearance of the foci when the upper and lower curly parts of the orbit appear.

The general solution of Eq. (7) is given by the following:

$$\Lambda_1 = \lambda_{1,2}^2 = \frac{-b + \sqrt{\Delta}}{2} \quad \Lambda_2 = \lambda_{3,4}^2 = \frac{-b - \sqrt{\Delta}}{2} \quad \hat{\boldsymbol{x}}_k = \begin{Bmatrix} 1 \\ u_k \\ \lambda_k \\ \lambda_k \cdot u_k \end{Bmatrix} \tag{8}$$

where λ_k are the eigenvalues, and $\hat{\boldsymbol{x}}_k$ are their corresponding eigenvectors for k varying from one to four. The HSP control proposed by Scheeres et al. aims to project the state position error along the eigenvectors direction associated to hyperbolic characteristic exponents [27]. This is done to guarantee the simple Lyapunov stability of the system. From a vectorial point of view, it is like defining a projection tensor given by $\boldsymbol{u}_k \boldsymbol{u}_k^T$ [27]. The first two normalized components of $\hat{\boldsymbol{x}}_k$ in Eq. (8) represent the unitary vector $\boldsymbol{u}_k$, and the expression of $\boldsymbol{u}_k$ is

$$\boldsymbol{u}_k = \frac{1}{\sqrt{1 + u_k \overline{u}_k}} \begin{bmatrix} 1 \\ u_k \end{bmatrix} \qquad u_k = \frac{\lambda_k^2 - V_{xx}}{V_{xy} + 2\omega_0 \lambda_k} \tag{9}$$

where $u_k \overline{u}_k$ is the product of u_k and its conjugate. Because the HSP control aims to stabilize the system in the sense of Lyapunov, the control law is designed to affect the sign of b, c, and Δ of Eq. (7). Indeed, the simple Lyapunov stability can be achieved by placing the eigenvalues of the linearized dynamics, the eigenvalues, on the imaginary axis, as shown in Fig. 4, by adding to V_{rr} an artificial potential, the center manifold T.

The artificial center manifold T is constructed from the linear combination of the projection tensors $\boldsymbol{u}_k \boldsymbol{u}_k^T$ and the gains. This linear combination is selected as b^c, c^c, and Δ^c, which are the indices of

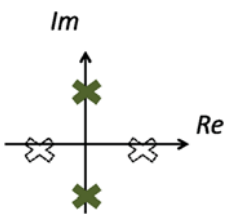

Fig. 4 Eigenvalues of the linearized dynamics with (filled crosses) and without (empty crosses) the effect of the HSP controller.

stability affected by the control law, which are all greater than zero [27]. The condition of simple Lyapunov stability is $\{b^c > 0 \,\&\, c^c > 0 \,\&\, \Delta^c > 0\}$, where the HSP control is added to the dynamics in Eq. (1) as an additional control acceleration $\boldsymbol{a}^c$ that will be modeled as SRP acceleration. Thus, $\boldsymbol{a}^c$ is given by the actuators model $\boldsymbol{a}^s$. Then, $\boldsymbol{a}^c$ is obtained by multiplying T by the state position error between the target orbit and the actual spacecraft trajectory $\delta \boldsymbol{r}$:

$$\boldsymbol{a}^c = T \delta \boldsymbol{r} \tag{10}$$

The acceleration $\boldsymbol{a}^c$ affects the linearized dynamics, and $Df(\overline{\boldsymbol{X}}(t))$ in Eq. (6) turns into $Df^c(\overline{\boldsymbol{X}}(t))$:

$$Df^c(\overline{\boldsymbol{X}}(t)) = \begin{bmatrix} \boldsymbol{0} & I \\ V_{rr}^c & 2\omega_0 \boldsymbol{J} \end{bmatrix} \tag{11}$$

The effect of the controller modifies V_{rr} into V_{rr}^c such that

$$V_{rr}^c = V_{rr} + T \tag{12}$$

In this work, the full formulation of the proposed extended HSP controller is derived for high-amplitude orbits. The control law designed by Scheeres et al. [27] is used when there is, along the orbit, a hyperbolic × center solution ($\Delta > 0$); Scheeres et al.'s control law is summarized in Sec. III.B. However, in the case of couples of complex and conjugate solutions ($\Delta < 0$), the dynamics requires a modified control law proposed by the authors of the present work in Sec. III.C.

A. Short-Term and Long-Term Stabilities

In this section, details are given to show the relationship between the short-term stability (shown in Fig. 4) and the long-term stability (shown in Fig. 2) [27]. Scheeres et al. [27] demonstrated that the short-term stability was an approximation of the long-term stability for a periodic linearized dynamical system:

$$\dot{\boldsymbol{x}} = A(t)\boldsymbol{x} A(t+T) = A(t), \qquad T > 0 \tag{13}$$

The stability of periodic orbit solutions (long-term stability shown in Fig. 2) can be studied in term of the Floquet multipliers. For a linear periodic system, the Floquet theorem [36] states the following: *Theorem 1 (Floquet theorem):* If $\Phi(t)$ is a fundamental matrix solution of the periodic system in Eq. (13), then so is $\Phi(t + T)$. Moreover, there exists an invertible periodic matrix $\boldsymbol{P}(t)$ with a T period such that

$$\Phi(t) = P(t) e^{Bt} \tag{14}$$

and B is a constant matrix.

Because $\Phi(t + T) = \Phi(t)\boldsymbol{C}$ with $\det \boldsymbol{C} \neq 0$ and $e^B = \boldsymbol{C}$, the eigenvalues ρ of $\boldsymbol{C}$ are called the characteristic multipliers of the periodic linear system. The eigenvalues λ of B are called the characteristic exponents of the periodic linear system where $\rho = e^{\lambda T}$.

LPOs have one pair of hyperbolic characteristic exponents and two circulation frequencies: one equal to the orbital period T, and one slightly longer. Because of the presence of the unstable manifold, uncontrolled relative motion to the target orbit will diverge in few orbital periods.

To maintain a long-term trajectory close to the target orbit, the spacecraft must be placed in the center manifold of the periodic orbit. However, the use of natural center manifolds is restrictive due to the unstable nature of the periodic orbit. Thus, the effect of the HSP control given along the trajectory aims to remove the instability by adding an artificial center manifold.

If we now focus on the short-term motion over a time much lower than the orbital period, although the description of the relative motion, Eq. (14) does not give a direct indication of the relative motion over a short time period. The state transition matrix Φ can be represented over one period as the product of mappings as follows [27]:

$$\Phi(t_0+T,t_0)=\prod_{i=1}^{N}\Phi\left[t_0+\frac{T}{N}i,t_0+\frac{T}{N}(i-1)\right] \tag{15}$$

where $\Delta t=T/N$ and $\Phi(t_i+\Delta t,t_i)$ satisfies the equation:

$$\dot{\Phi}(t_i+\delta t,t_i)=A(t_i+\delta t)\Phi(t_i+\delta t,t_i)0\le\delta t\le\Delta t\ll T \tag{16}$$

For small Δt, the matrix $A(t)$ can be expanded in a Taylor series. Scheeres et al. [27] found that, for periodic orbits around the libration point, $\dot{A}(t_i)$ does not vary strongly over the time. This means that Δt can be chosen small enough to ensure that $\|A(t_i)\|\gg\|\dot{A}(t_i)\Delta t\|$. Under this restriction, Scheeres et al. [27] found that the state transition matrix differential equation can be approximated over short-time intervals as follows:

$$\Phi(t_i+\delta t,t_i)\sim I+A(t_i)\delta t+\ldots \tag{17}$$

Note that series expansion of the higher-order terms is neglected because the time interval is chosen to be sufficiently small. Equation (17) is commonly used in a discrete-time model, which is the Euler model, which is a first-order numerical approximation of the continuous-time dynamics. The relative motion can be finally characterized over a short period of time as follows [27]:

$$(\lambda I-\Phi)\boldsymbol{u}=0 \tag{18}$$

where λ is the eigenvalue, and $\boldsymbol{u}$ is the eigenvector. By substituting Eqs. (17) and (18), this can be written as follows:

$$\left(\frac{(\lambda-1)}{\delta t}I-A(t_i)\right)\boldsymbol{u}=0 \tag{19}$$

For a time-invariant system, the eigenvalue of the state transition matrix λ is equal to $e^{\gamma\cdot\delta t}$, and γ is the characteristic exponent of the system. The eigenvalues of Eq. (19) can be approximated as follows:

$$\gamma\sim\lim_{\delta t\to 0}\frac{\lambda-1}{\delta t} \tag{20}$$

Under these approximations, the relative motion over a short time can be understood by analyzing the eigenstructure of the matrix $A(t_i)$. The error induced by this approximation was investigated by Scheeres et al. [27] and is shown to be reasonable. Scheeres et al. [27] derived the HSP control law by using the short-term dynamics to guide the understanding of the stability. The relative motion along the instantaneous unstable manifold is seen as a precursor to the motion along the unstable manifold of the full orbit, as defined by the Floquet theory. Note that the full orbit may still be unstable even if the instantaneous map is stable at each time step.

As previously said, the stabilization of the relative motion over a short time is a necessary but not sufficient condition to ensure that the motion of the spacecraft will be stable over a long time span. The conditions to reach the stability were presented by Scheeres et al. [27]. The stability of the system can, however, be evaluated by application of the Floquet theory and numerical integration.

The stability is evaluated as follows. The periodic orbit and its associated state transition matrix modified by adding the effect of the control is numerically integrated over one period of motion. At each time step, we compute the linear equations as follows:

$$\delta\dot{\overline{\boldsymbol{X}}}(t)=A^c(\overline{\boldsymbol{X}}(t))\delta\overline{\boldsymbol{X}}(t) \tag{21}$$

where $A^c(\overline{\boldsymbol{X}}(t))$ is defined as in Eq. (11) and is the time-varying matrix used in the state transition matrix computation. The resulting state transition matrix is denoted as $\Phi^c(t_0+t,t_0)$, and the monodromy matrix evaluated over one period of motion is $\Phi^c(t_0+T,t_0)$. The stability of the closed-loop system can be evaluated by computing the eigenvalues μ (the monodromy matrix) as follows:

$$|\mu I-\Phi^c(t_0+T,t_0)|=0 \tag{22}$$

As is well known, these eigenvalues must occur in complex and conjugate pairs, as well as in inverse pairs. Stability of this system occurs when all eigenvalues have a unit magnitude that corresponds to the unit circle in the complex plane and have the form $\mu=e^{\pm i\theta}$, as shown in Fig. 2.

B. Control Law for Local Hyperbolic × Center Equilibrium

In this section, the control law proposed by Scheeres et al. [27] is summarized because this control law is used in case of local hyperbolic × center equilibrium (i.e., low-amplitude orbits); see Fig. 5.

Moreover, it is useful to compare this formulation with the proposed control law for complex and conjugate roots (in Sec. III.C) in order to understand the main differences. The hyperbolic characteristic exponents for the stable λ_1 and unstable λ_2 directions are the solutions of the linearized dynamics in Eq. (8) where, now, the real roots $\lambda_{1,2}$ are named as $\pm\sigma$. The corresponding eigenvector to σ is

$$\begin{aligned}\boldsymbol{u}_1&=\frac{1}{\sqrt{1+u_1^2}}\begin{bmatrix}1\\u_1\end{bmatrix}\qquad u_1=\frac{\sigma^2-V_{xx}}{V_{xy}+2\omega_0\sigma}\\ \boldsymbol{u}_1\boldsymbol{u}_1^T&=\frac{1}{1+u_1^2}\begin{bmatrix}1&u_1\\u_1&u_1^2\end{bmatrix}\end{aligned} \tag{23}$$

where u_1 is real, and such that the projection tensor $\boldsymbol{u}_1\boldsymbol{u}_1^T$ is real. The corresponding eigenvector to $-\sigma$ is instead

$$\begin{aligned}\boldsymbol{u}_2&=\frac{1}{\sqrt{1+u_2^2}}\begin{bmatrix}1\\u_2\end{bmatrix}\qquad u_2=\frac{\sigma^2-V_{xx}}{V_{xy}-2\omega_0\sigma}\\ \boldsymbol{u}_2\boldsymbol{u}_2^T&=\frac{1}{1+u_2^2}\begin{bmatrix}1&u_2\\u_2&u_2^2\end{bmatrix}\end{aligned} \tag{24}$$

where u_2 is real and the projection tensor $\boldsymbol{u}_2\boldsymbol{u}_2^T$ is real. The control law proposed by Scheeres et al. [27] is then

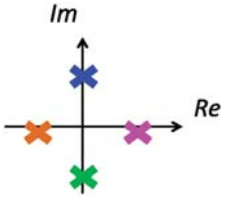

Fig. 5 Couples of real and pure imaginary eigenvalues of the linearized equations: λ_1 (rightmost cross), λ_2 (leftmost cross), λ_3 (top cross), and λ_4 (bottom cross).

$$\boldsymbol{a}^c = -\sigma^2 G_1[\boldsymbol{u}_1\boldsymbol{u}_1^T + \boldsymbol{u}_2\boldsymbol{u}_2^T]\delta\boldsymbol{r} \tag{25}$$

As said, the validity of the control law in Eq. (25) is for solutions where the instantaneous stability map has two couples of real and pure imaginary eigenvalues. This is the case for low-amplitude LPOs.

C. Control Law for Complex and Conjugate Pairs

When couples of complex and conjugate numbers occur, as in the case of high-amplitude orbits, the eigenvalues are the solution of the linear system in Eq. (8) where, now, $\lambda_{1,2,3,4}$ are complex and conjugate pairs; thus, now, $\lambda_{1,2}$ and $\lambda_{3,4}$ are $\pm(\sigma+\gamma i)$ and $\pm(\sigma-\gamma i)$, respectively, as shown in Fig. 6. The idea proposed here for the design of the extended control law is to get rid of the imaginary components in order to have a real control acceleration. Thus, the eigenvector components are separately analyzed in order to highlight possible conjugate terms for the design of the eigenvectors normalization and the control acceleration. Starting from $\lambda_1 = \sigma + \gamma i$, its correspondent eigenvector component u_1 is

$$u_1 = \frac{\sigma^2 - V_{xx} - \gamma^2 + 2\sigma\gamma i}{V_{xy} + 2\omega_0\sigma + 2\omega_0\gamma i} = \frac{A_1 + B_1 i}{C_1 + D_1 i} \tag{26}$$

that, after mathematical manipulation, can be written as follows:

$$u_1 = \frac{(A_1C_1 + B_1D_1) - (A_1D_1 - B_1C_1)i}{C_1^2 + D_1^2} \quad \begin{cases} A_1 = \sigma^2 - V_{xx} - \gamma^2 \\ B_1 = 2\sigma\gamma \\ C_1 = V_{xy} + 2\omega_0\sigma \\ D_1 = 2\omega_0\gamma \end{cases} \tag{27}$$

The same approach can be used for $\lambda_2 = -\sigma - \gamma i$, where the correspondent eigenvector component is defined as

$$u_2 = \frac{\sigma^2 - V_{xx} - \gamma^2 + 2\sigma\gamma i}{V_{xy} - 2\omega_0\sigma - 2\omega_0\gamma i} = \frac{A_2 + B_2 i}{C_2 - D_2 i} \tag{28}$$

Thus, it is possible to highlight the real and imaginary parts of u_2 as

$$u_2 = \frac{(A_2C_2 - B_2D_2) + (A_2D_2 + B_2C_2)i}{C_2^2 + D_2^2} \quad \begin{cases} A_2 = \sigma^2 - V_{xx} - \gamma^2 \\ B_2 = 2\sigma\gamma \\ C_2 = V_{xy} - 2\omega_0\sigma \\ D_2 = 2\omega_0\gamma \end{cases} \tag{29}$$

As before, the correspondent eigenvector component u_3 to $\lambda_3 = \sigma - \gamma i$ is

$$u_3 = \frac{\sigma^2 - V_{xx} - \gamma^2 - 2\sigma\gamma i}{V_{xy} + 2\omega_0\sigma - 2\omega_0\gamma i} = \frac{A_3 - B_3 i}{C_3 - D_3 i} \tag{30}$$

and, by manipulating the previous expression, it is possible to write

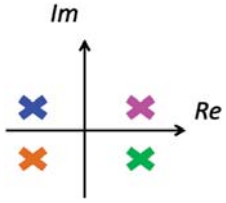

Fig. 6 Couples of complex and conjugate eigenvalues of the linearized equations: λ_1 (upper-right cross), λ_2 (lower-left cross), λ_3 (lower-right cross), and λ_4 (upper-left cross).

$$u_3 = \frac{(A_3C_3 + B_3D_3) + (A_3D_3 - B_3C_3)i}{C_2^2 + D_2^2} \quad \begin{cases} A_3 = \sigma^2 - V_{xx} - \gamma^2 \\ B_3 = 2\sigma\gamma \\ C_3 = V_{xy} + 2\omega_0\sigma \\ D_3 = 2\omega_0\gamma \end{cases} \tag{31}$$

Finally, in the case of $\lambda_4 = -\sigma + \gamma i$, the correspondent eigenvector component is u_4:

$$u_4 = \frac{\sigma^2 - V_{xx} - \gamma^2 - 2\sigma\gamma i}{V_{xy} - 2\omega_0\sigma + 2\omega_0\gamma i} = \frac{A_4 - B_4 i}{C_4 + D_4 i} \tag{32}$$

and it can be defined as

$$u_4 = \frac{(A_4C_4 - B_4D_4) - (A_4D_4 + B_4C_4)i}{C_4^2 + D_4^2} \quad \begin{cases} A_4 = \sigma^2 - V_{xx} - \gamma^2 \\ B_4 = 2\sigma\gamma \\ C_4 = V_{xy} - 2\omega_0\sigma \\ D_4 = 2\omega_0\gamma \end{cases} \tag{33}$$

By noticing that

$$\begin{cases} A_1 = A_2 = A_3 = A_4 = A = \sigma^2 - V_{xx} - \gamma^2 \\ B_1 = B_2 = B_3 = B_4 = B = 2\sigma\gamma \\ C_1 = C_3 = C = V_{xy} + 2\omega_0\sigma \\ C_2 = C_4 = \overline{C} = V_{xy} - 2\omega_0\sigma \\ D_1 = D_2 = D_3 = D_4 = D = 2\omega_0\gamma \end{cases} \tag{34}$$

it is possible to rewrite the expression of u_k, with k defined from one to four, as follows:

$$u_1 = \frac{(AC + BD) - (AD - BC)i}{C^2 + D^2} \quad u_2 = \frac{(A\overline{C} - BD) + (AD + B\overline{C})i}{\overline{C}^2 + D^2} \tag{35}$$

$$u_3 = \frac{(AC + BD) + (AD - BC)i}{C^2 + D^2} \quad u_4 = \frac{(A\overline{C} - BD) - (AD + B\overline{C})i}{\overline{C}^2 + D^2} \tag{36}$$

So, u_1 and u_3 are complex and conjugate, and u_2 and u_4 are complex and conjugate as well. Moreover, if a change of variables is applied,

$$\begin{cases} a_* = AC + BD \\ b_* = AD - BC \\ c_* = C^2 + D^2 \\ d_* = A\overline{C} - BD \\ e_* = AD + B\overline{C} \\ f_* = \overline{C}^2 + D^2 \end{cases} \tag{37}$$

it is possible to define the eigenvectors and their normalizations by knowing that u_3 is the conjugate of u_1 and u_4 is the conjugate of u_2:

$$\boldsymbol{u_1} = \frac{1}{\sqrt{1 + u_1u_3}}\begin{bmatrix} 1 \\ u_1 \end{bmatrix} \qquad u_1 = \frac{a_* - b_* i}{c_*} \tag{38}$$

$$\boldsymbol{u_3} = \frac{1}{\sqrt{1 + u_1u_3}}\begin{bmatrix} 1 \\ u_3 \end{bmatrix} \qquad u_3 = \frac{a_* + b_* i}{c_*} \tag{39}$$

$$\boldsymbol{u_2} = \frac{1}{\sqrt{1 + u_2u_4}}\begin{bmatrix} 1 \\ u_2 \end{bmatrix} \qquad u_2 = \frac{d_* + e_* i}{f_*} \tag{40}$$

$$\boldsymbol{u_4} = \frac{1}{\sqrt{1 + u_2u_4}}\begin{bmatrix} 1 \\ u_4 \end{bmatrix} \qquad u_4 = \frac{d_* - e_* i}{f_*} \tag{41}$$

where a_*, b_*, c_*, d_*, e_*, and f_* are functions of the eigenvalues and V_{rr}:

$$\begin{cases} a_* = (\sigma^2 - V_{xx} - \gamma^2)(V_{xy} + 2\omega_0\sigma) + (2\sigma\gamma)(2\omega_0\gamma) \\ b_* = (\sigma^2 - V_{xx} - \gamma^2)(2\omega_0\gamma) - (2\sigma\gamma)(V_{xy} + 2\omega_0\sigma) \\ c_* = (V_{xy} + 2\omega_0\sigma)^2 + (2\omega_0\gamma)^2 \\ d_* = (\sigma^2 - V_{xx} - \gamma^2)(V_{xy} - 2\omega_0\sigma) - (2\sigma\gamma)(2\omega_0\gamma) \\ e_* = (\sigma^2 - V_{xx} - \gamma^2)(2\omega_0\gamma) + (2\sigma\gamma)(V_{xy} - 2\omega_0\sigma) \\ f_* = (V_{xy} - 2\omega_0\sigma)^2 + (2\omega_0\gamma)^2 \end{cases} \tag{42}$$

Because u_1 and u_3 are complex and conjugate and u_2 and u_4 are complex and conjugate, we can write a new control law for high-amplitude orbits as follows. From the normalization, we know that

$$u_1 u_3 = (a_* - b_* i) \cdot (a_* + b_* i) = a_*^2 + b_*^2 \tag{43}$$

and

$$u_2 u_4 = (d_* + e_* i) \cdot (d_* - e_* i) = d_*^2 + e_*^2 \tag{44}$$

The four projection tensors are now defined as follows:

$$\boldsymbol{u}_1\boldsymbol{u}_1^T = \frac{1}{1 + u_1 u_3}\begin{bmatrix} 1 & u_1 \\ u_1 & u_1^2 \end{bmatrix}, \quad \boldsymbol{u}_3\boldsymbol{u}_3^T = \frac{1}{1 + u_1 u_3}\begin{bmatrix} 1 & u_3 \\ u_3 & u_3^2 \end{bmatrix} \tag{45}$$

$$\boldsymbol{u}_2\boldsymbol{u}_2^T = \frac{1}{1 + u_2 u_4}\begin{bmatrix} 1 & u_2 \\ u_2 & u_2^2 \end{bmatrix}, \text{ and } \boldsymbol{u}_4\boldsymbol{u}_4^T = \frac{1}{1 + u_2 u_4}\begin{bmatrix} 1 & u_4 \\ u_4 & u_4^2 \end{bmatrix} \tag{46}$$

It is interesting to note that the only linear combination among the projection tensors that guarantees a real control law requires the couples of the projection tensors to be weighted with the same gain. This can be demonstrated by looking at $\boldsymbol{u}_k$ and u_k in Eqs. (38–41). The only solution is to keep the tensors associated to $\boldsymbol{u}_1$ and $\boldsymbol{u}_3$ with the same gain such that

$$\boldsymbol{u}_1\boldsymbol{u}_1^T + \boldsymbol{u}_3\boldsymbol{u}_3^T = \frac{1}{1 + u_1 u_3}\begin{bmatrix} 1 & u_1 + u_3 \\ u_1 + u_3 & u_1^2 + u_3^2 \end{bmatrix} \tag{47}$$

$$u_1 + u_3 = a_* - b_* i + a_* + b_* i = 2a_* \tag{48}$$

and

$$u_1^2 + u_3^2 = (a_* - b_* i)^2 + (a_* + b_* i)^2 = 2(a_*^2 - b_*^2) \tag{49}$$

are all real. For the same reason, the tensors associated to $\boldsymbol{u_2}$ and $\boldsymbol{u_4}$ should be weighted with the same gain to achieve a real control acceleration. So,

$$\boldsymbol{u}_2\boldsymbol{u}_2^T + \boldsymbol{u}_4\boldsymbol{u}_4^T = \frac{1}{1 + u_2 u_4}\begin{bmatrix} 1 & u_2 + u_4 \\ u_2 + u_4 & u_2^2 + u_4^2 \end{bmatrix} \tag{50}$$

$$u_2 + u_4 = d_* + e_* i + d_* - e_* i = 2d_* \tag{51}$$

and

$$u_2^2 + u_4^2 = (d_* + e_* i)^2 + (d_* - e_* i)^2 = 2(d_*^2 - e_*^2) \tag{52}$$

are real terms too. The proposed control law for high-amplitude orbits needs to be weighted with the same gain couples of complex and conjugate eigenvectors in order to have a real control acceleration and to cancel the imaginary parts out:

$$\boldsymbol{a}^c = \{-\lambda_1\lambda_3 G_1[\boldsymbol{u}_1\boldsymbol{u}_1^T + \boldsymbol{u}_3\boldsymbol{u}_3^T] - \lambda_2\lambda_4 G_2[\boldsymbol{u}_2\boldsymbol{u}_2^T + \boldsymbol{u}_4\boldsymbol{u}_4^T]\}\delta\boldsymbol{r} \tag{53}$$

where

$$\begin{aligned} \lambda_1\lambda_3 &= (\sigma + \gamma i)(\sigma - \gamma i) = \sigma^2 + \gamma^2\lambda_2\lambda_4 \\ &= (-\sigma - \gamma i)(-\sigma + \gamma i) = \sigma^2 + \gamma^2 \end{aligned} \tag{54}$$

are all real and positive numbers. Thus, $\boldsymbol{a}^c$ can be further simplified to

$$\boldsymbol{a}^c = -(\sigma^2 + \gamma^2)\Big\{G_2[\boldsymbol{u}_1\boldsymbol{u}_1^T + \boldsymbol{u}_3\boldsymbol{u}_3^T] + G_3[\boldsymbol{u}_2\boldsymbol{u}_2^T + \boldsymbol{u}_4\boldsymbol{u}_4^T]\Big\}\delta\boldsymbol{r} \tag{55}$$

In conclusion, the HSP control algorithm is designed such that

$$\boldsymbol{a}^c = \begin{cases} \text{Eq.(25)} & \text{if } \Delta > 0 \text{ Scheeres et al. [27]} \\ \text{Eq.(55)} & \text{if } \Delta < 0 \end{cases} \tag{56}$$

The proposed control in Eq. (56) was implemented in the CRUISE (which stands for controlled routes by using innovative solar-radiation equipment) algorithm in MATLAB language. An important remark is that not all the gain sets (G_1, G_2, and G_3) can stabilize the orbit because the local stability is not a necessary condition of the periodic orbit stability due to resonance effects [27].

IV. Gain Definition to Achieve Simple Lyapunov Stability

The simple stability is guaranteed for the following:

$$\begin{cases} b^c = 4\omega^2 - V_{xx}^c - V_{yy}^c > 0 \\ c^c = V_{xx}^c V_{yy}^c - (V_{xy}^c)^2 > 0 \\ \Delta^c = (b^c)^2 - 4c^c > 0 \end{cases} \tag{57}$$

The linear stability was already proven by Scheeres et al. [27] for the hyperbolic × center solution; in this case, G_1 in Eq. (25) should be selected to be large enough to guarantee linear stability. In this section, a similar approach is used to study the stability as a function of G_2 and G_3 associated to the extended control in Eq. (55), where complex and conjugate eigenvalues occur. For the definition of the control law in Eq. (55), V_{xx}^c, V_{yy}^c, and V_{xy}^c are defined as follows:

$$V_{xx}^c = V_{xx} - G_2\frac{(\sigma^2 + \gamma^2)}{1 + u_1 u_3} - G_3\frac{(\sigma^2 + \gamma^2)}{1 + u_2 u_4} \tag{58}$$

$$V_{yy}^c = V_{yy} - G_2\frac{(\sigma^2 + \gamma^2)(u_1^2 + u_3^2)}{1 + u_1 u_3} - G_3\frac{(\sigma^2 + \gamma^2)(u_2^2 + u_4^2)}{1 + u_2 u_4} \tag{59}$$

$$V_{xy}^c = V_{xy} - G_2\frac{(\sigma^2 + \gamma^2)(u_1 + u_3)}{1 + u_1 u_3} - G_3\frac{(\sigma^2 + \gamma^2)(u_2 + u_4)}{1 + u_2 u_4} \tag{60}$$

The definition of b^c is

$$b^c = b + (\sigma^2 + \gamma^2)\left[G_2\frac{1 + u_1^2 + u_3^2}{1 + u_1 u_3} + G_3\frac{1 + u_2^2 + u_4^2}{1 + u_4 u_4}\right] \tag{61}$$

Because $b < 0$ and b^c must be greater than zero, it is important to study the sign of the terms associated to the controller. In Eq. (61), $u_1 u_3 = a_*^2 + b_*^2$ and $u_2 u_4 = d_*^2 + e_*^2$ are positive terms; thus, all the fractions are positive (greater than zero). This means that, for the first condition in Eq. (57), G_2 and G_3 should be positive and big enough to keep $b^c > 0$. As a consequence of Eq. (57), $(b^c)^2$ must be greater than $4c^c$ such that $\Delta^c > 0$. The definition of Δ^c is

$$\Delta^c = (4\omega^2 - V_{xx}^c - V_{yy}^c)^2 - 4(V_{xx}^c V_{yy}^c - (V_{xy}^c)^2) \tag{62}$$

where Eq. (62) can be rewritten as follows:

$$\Delta^c = 8\omega^2 b^c + (V^c_{xx} - V^c_{yy})^2 + 4(V^c_{xy})^2 \tag{63}$$

Because $(V^c_{xx} - V^c_{yy})^2$ and $(V^c_{xy})^2$ are positive terms, the condition $\Delta^c > 0$ is satisfied by $b^c > 0$. The definition of c^c is

$$c^c = c + (\sigma^2+\gamma^2)^2\left[G_2^2\frac{u_1^2+u_3^2}{(1+u_1u_3)^2} + G_3^2\frac{u_2^2+u_4^2}{(1+u_2u_4)^2} + \frac{G_2G_3(u_2^2+u_4^2+u_1^2+u_3^2)}{(1+u_2u_4)(1+u_1u_3)}\right] + K_n \tag{64}$$

where K_n are all the negative terms:

$$K_n = -(\sigma^2+\gamma^2)\left\{G_2\left[\frac{V_{xx}(u_1^2+u_3^2)+V_{yy}}{1+u_1u_3} - \frac{2V_{xy}(u_1+u_3)}{1+u_1u_3} + G_2(\sigma^2+\gamma^2)\frac{(u_1+u_3)^2}{(1+u_1u_3)^2}\right] + G_3\left[\frac{V_{xx}(u_2^2+u_4^2)+V_{yy}}{1+u_2u_4} - \frac{2V_{xy}(u_2+u_4)}{1+u_2u_4} + G_3(\sigma^2+\gamma^2)\frac{(u_2+u_4)^2}{(1+u_2u_4)^2}\right] + 2G_2G_3(\sigma^2+\gamma^2)\frac{(u_1+u_3)(u_2+u_4)}{(1+u_2u_4)(1+u_1u_3)}\right\} \tag{65}$$

Because $c < 0$, K_n collects all the negative terms, c^c must be greater than zero, and G_2 and G_3 must be positive and big enough to guarantee the stability. Note that, as a result of both conditions of $b^c > 0$ and $c^c > 0$, either G_2 or G_3 must be nonzero. This qualitative analysis gives an understanding on how to select the gains. However, it does not give quantitative information. Examples of optimization techniques that can be used to select the control gains were shown in [37,38]

V. Actuators Model: Deployable Reflective Structures

As shown by Farrés and Jorba [23] and Xu and Xu [28], the HSP control acceleration can be expressed with the linear approximation in the orientation angles and area, so $\boldsymbol{a}^s$ is defined as follows:

$$\boldsymbol{a}^s(\alpha,\delta,\beta) = \boldsymbol{a}^s(\alpha_0,\delta_0,\beta_0) + \left.\frac{\partial \boldsymbol{a}^s}{\partial\alpha}\right|_{(\alpha_0,\delta_0,\beta_0)}(\alpha-\alpha_0) + \left.\frac{\partial \boldsymbol{a}^s}{\partial\delta}\right|_{(\alpha_0,\delta_0,\beta_0)}(\delta-\delta_0) + \left.\frac{\partial \boldsymbol{a}^s}{\partial\beta}\right|_{(\alpha_0,\delta_0,\beta_0)}(\beta-\beta_0) + O(2) \tag{66}$$

Then, it is possible to write $\Delta\alpha = (\alpha-\alpha_0)$, $\Delta\delta = (\delta-\delta_0)$, and $\Delta\beta = (\beta-\beta_0)$; by imposing that the SRP acceleration is given by the HSP control as $\boldsymbol{a}^s(\alpha,\delta,\beta) = \boldsymbol{a}^c$, Eq. (66) can be rewritten as follows:

$$\boldsymbol{a}^c = \boldsymbol{a}^s(\alpha_0,\delta_0,\beta_0) + \left.\left[\frac{\partial \boldsymbol{a}^s}{\partial\boldsymbol{\Theta}}\right]\right|_{(\alpha_0,\delta_0,\beta_0)}\Delta\boldsymbol{\Theta} + O(2) \tag{67}$$

where $\Delta\boldsymbol{\Theta}$ is defined such as $\{\Delta\alpha, \Delta\delta, \Delta\beta\}^T$, and the Jacobian matrix is defined as follows:

$$\left.\left[\frac{\partial \boldsymbol{a}^s}{\partial\boldsymbol{\Theta}}\right]\right|_{(\alpha_0,\delta_0,\beta_0)} = \left[\left.\frac{\partial \boldsymbol{a}^s}{\partial\alpha}\right|_{(\alpha_0,\delta_0,\beta_0)}, \left.\frac{\partial \boldsymbol{a}^s}{\partial\delta}\right|_{(\alpha_0,\delta_0,\beta_0)}, \left.\frac{\partial \boldsymbol{a}^s}{\partial\beta}\right|_{(\alpha_0,\delta_0,\beta_0)}\right] \tag{68}$$

The derivatives of the SRP acceleration in Eq. (68) is given in Appendix B; by inverting Eq. (67), the variation in the control parameters is given by

$$\Delta\boldsymbol{\Theta} = \left.\left[\frac{\partial \boldsymbol{a}^s}{\partial\boldsymbol{\Theta}}\right]^{-1}\right|_{(\alpha_0,\delta_0,\beta_0)}(\boldsymbol{a}^c - \boldsymbol{a}^s(\alpha_0,\delta_0,\beta_0)) \tag{69}$$

VI. Study of Stability with the Effect of the SRP Acceleration

In this section, the performance of the HSP control when used with SRP acceleration will be investigated, where the control acceleration is given by the actuator model shown in Sec. V, and the control law proposed by McInnes [22]. McInnes's work was based on a trajectory station-keeping technique proposed by Howell and Pernicka [20] (the target point approach) and modified by McInnes [22] such that the maneuvers were given by the effect of SRP acceleration when changing the sail orientation angles. To allow the comparison, we extended the work of McInnes to also include changes in the lightness parameter β. Thus, the variational equations can be written as follows:

$$\frac{\mathrm{d}}{\mathrm{d}t}\begin{bmatrix}\delta\boldsymbol{r}\\ \delta\dot{\boldsymbol{r}}\\ \delta\boldsymbol{s}\end{bmatrix} = \begin{bmatrix}\boldsymbol{0} & I & \boldsymbol{0}\\ V_{rr} & 2\omega_0\boldsymbol{J} & \boldsymbol{a}^s_{rs}\\ \boldsymbol{0} & \boldsymbol{0} & \boldsymbol{0}\end{bmatrix}\begin{bmatrix}\delta\boldsymbol{r}\\ \delta\dot{\boldsymbol{r}}\\ \delta\boldsymbol{s}\end{bmatrix} \tag{70}$$

where, as for Eq. (6), $\delta\boldsymbol{r}$ is the position error with respect to the target orbit, $\delta\dot{\boldsymbol{r}}$ is the velocity error with respect to the target, $\boldsymbol{J}$ is defined as in Eq. (6), and $\delta\boldsymbol{s} = \{\alpha,\delta,\beta\}$ is the vector of the control parameters in terms of the SRP angles and lightness parameter. Note that Eqs. (6) and (70) differ only for the selected states variables; however, here, the SRP control parameters $\delta\boldsymbol{s}$ are included in the state. The target point algorithm is written in term of a cost function that contains the deviation of the actual trajectory given by

$$\delta\bar{x}(t) = \Phi(t,t_0)\cdot\delta\bar{x}(t_0) \tag{71}$$

where Φ is the state transition matrix, which is now affected by the SRP acceleration. The deviation from the actual trajectory is then used to design the target point cost function (for further details, refer to [20,22]). The aim here is not to derive the target point algorithm but to study the Lyapunov stability of Eq. (70). We aim to demonstrate that the effect of the SRP acceleration in the target point algorithm in Eq. (70) does not affect the local stability when compared to the HSP control, where Df^c is defined as in Eq. (11). However, the orbit stability is affected by SRP acceleration because the target point control modifies the state transition matrix. The idea is to study the stability of this new linearized equations, where the characteristic polynomial is given by computing the determinant of $D(\lambda) = |Df^c - \lambda I| = 0$ where, here, Df^c is defined as the matrix in Eq. (70). For the planar dynamics, the characteristic polynomial is found to be

$$\Lambda^2 + (4 - V_{xx} - V_{yy})\Lambda + (V_{xx}V_{yy} - V_{xy}^2) = 0 \tag{72}$$

From Eq. (72), it becomes clear that these modified linearized equations do not affect the local behavior of the system because we found the same characteristic polynomial as the planar case without the effect of SRP acceleration in Eq. (7). Thus, changing the angles or β will not stabilize the system and the system will still have hyperbolic × center eigenvalues or couples of complex and conjugate values. The simple Lyapunov stability cannot be reached; thus, an artificial potential that affects the sign of b, c, and Δ is needed as for the HSP control. However, note that the eigenvalues of the monodromy matrix are affected by the SRP acceleration. Thus, the target point approach cannot guarantee Lyapunov stability.

VII. Hamiltonian Structure-Preserving Control Through Solar Radiation Pressure Actuators

The purpose of this study is to investigate the use of SRP for station keeping of spacecraft in high-amplitude DPOs. The selected orbits are high-amplitude DPOs (in Fig. 3a) and planar-Lyapunov orbits, shown in Fig. 3b. When SRP is incorporated, in order to have a feasible acceleration, the values of the unstable manifold should never be negative (i.e., the spacecraft escaping outward from the sun). Goméz et al. [19] named this peculiarity the "always towards the sun rule." This effect causes saturation in the actuator system when the lightness parameter β is constrained between zero and one, and the orientation angles should be limited between $-\pi/2$ and $+\pi/2$ in both

Table 1 Area and orientations angles required for different initial reflective areas and injection errors

x-axis offset, km	A^0, m^2	β_0	A, m^2	β	α, deg	δ, deg
−40	10	$1.53 \cdot 10^{-5}$	— —	— —	— —	— —
−40	20	$3.06 \cdot 10^{-5}$	— —	— —	— —	— —
−5	20	$3.06 \cdot 10^{-5}$	15.5–21.5	$2.4 \cdot 10^{-5}$–$3.29 \cdot 10^{-5}$	±2.5	$\pm 7 \cdot 10^{-3}$
−40	30	$4.59 \cdot 10^{-5}$	— —	— —	— —	— —
−40	35	$5.355 \cdot 10^{-5}$	0.5–47	$1.306 \cdot 10^{-6}$–$7.24 \cdot 10^{-5}$	±10.5	±3
−40	40	$6.12 \cdot 10^{-5}$	5.5–52.32	$8.331 \cdot 10^{-6}$–$8.004 \cdot 10^{-5}$	±9.5	±2.5
−40	70	$1.071 \cdot 10^{-4}$	35–83.3	$5.436 \cdot 10^{-5}$–$1.259 \cdot 10^{-4}$	±5.5	±1.5
0	70	$1.071 \cdot 10^{-4}$	69.99–70.0001	$1.071 \cdot 10^{-4}$	$\pm 2.635 \cdot 10^{-5}$	$\pm 7.5 \cdot 10^{-8}$
−40	100	$1.53 \cdot 10^{-4}$	65.66–112	$1.004 \cdot 10^{-4}$–$1.718 \cdot 10^{-4}$	±3.8	±1.02

α and δ. Gómez et al. explained that this effect could not be overcome unless a very high area-to-mass ratio was used. A previous extension of HSP with SRP proposed by Xu and Xu [28] fulfilled the always-towards–the-sun rule by selecting a very high area-to-mass ratio to avoid saturation in the control parameters. Xu and Xu [28] selected a Lissajous orbit to apply their control law, and they used an initial lightness parameter β_0 of 0.5059 that, for a spacecraft with the same mass as SOHO, corresponded to an initial area of $6.1270 \cdot 10^5$ m^2 (which was equivalent to a 782.75 m span of a square sail area). Recently, the Japan Aerospace Exploration Agency's IKAROS mission demonstrated the capability to deploy a 20-m-span sail [39]; thus, this size of area required, as an example, for SOHO is infeasible with current technology. As our study aims to understand which parameters affect the pointing requirements and the size of the actuator area for high-amplitude orbits, we first analyze the structural requirements for the simple case of halo orbits (relevant to the SOHO mission), where the SRP acceleration is provided by the HSP control law designed by Scheeres et al. [27].

A. SOHO Mission Scenario

In this section, SOHO is used as a mission scenario to verify when SRP is a feasible option to control a spacecraft in a halo orbit using the HSP controller. In this case, the control works in the regime of the hyberbolic equilibrium and a gain of $G_1 = 10$ is required to stabilize the orbit. The mass of SOHO is set to 1000 kg, and the required control parameters are in terms of the reflective area A, in-plane angle α, and out-of-plane angle δ. These are computed as a function of the injection error and the initial reflective area of the spacecraft. The spacecraft is originally sun pointing before the action of the HSP controller. The controller is tested for a maximum of nine orbital periods that correspond to 4.4 years.

The results are shown in Table 1, where it can be seen that high injection errors require a higher initial area A_0 to guarantee a feasible solution. For example, Fig. 7 shows the case of $A_0 = 20$ m^2 and an offset of −40 km. The solution is not feasible because of the requirements of a negative area; thus, for this specific initial injection error, a minimum of 35 m^2 in A_0 is required to have a feasible area, as shown in Table 1. In the case of no error in the halo orbit insertion maneuver, the pointing requirements and the area needed to control the spacecraft are very tiny, as shown in Table 1 for the case of $A_0 = 70$ m^2. This shows that the HSP control requires very few accelerations to stabilize the orbit. This is confirmed by Fig. 8, which compares the same case scenario with (Figs. 8a, 8c, and 8e) and without (Figs. 8b, 8d, and 8f) an initial injection error. Note that, when the injection error is not considered, the controller acceleration is zero at the first orbital period because the spacecraft is exactly placed onto the target orbit. Table 1 shows that, for $A_0 = 20$ m^2 and an injection error of −5 km, the solution exists and it requires reasonable variations in the area required and in the orientation angles. It also shows that, in this case, the controller should be limited to variations in just the area and the in-plane angle α because the variations in the out-of-plane angle $\boldsymbol{\delta}$ are very tiny; thus, they are not feasible.

These results suggest that the HSP controller is a good candidate to perform propellant-free control using SRP acceleration. The initial area required depends on the initial injection error; however, an initial offset is required to avoid tiny control requirements that cannot be physically achieved. For example, an offset of −5 km from the target orbit requires an initial area of 20 m^2 with variations of the area of 15.5–21.5 m^2, as shown in Table 1. The pointing requirements are feasible in α, on the order of magnitude of the telescopes' sunshade pointing requirements for LPOs; whereas, in this case in δ, a control action is not necessary.

Note that the continuous acceleration requires the design of a variable-geometry actuator system; thus, the control acceleration should be limited in the variations of the control area required. It is thus recommended to investigate a HSP control discrete in time to avoid a continuous change of the reflective area.

B. High-Amplitude Planar DPOs and LPOs

In this section, the performance of the HSP controller enhanced by SRP is tested for high-amplitude orbits where a couple of complex

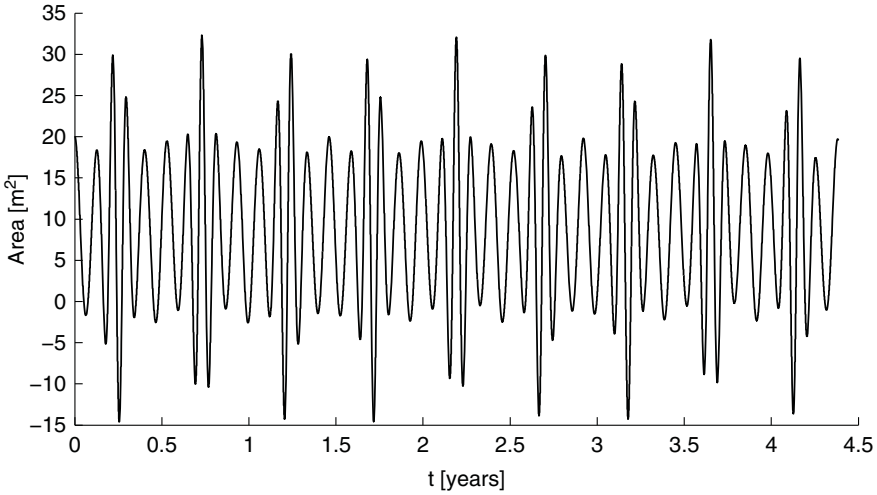

Fig. 7 Required area when the initial area is m^2 and an initial offset in x of −40 km is taken into account.

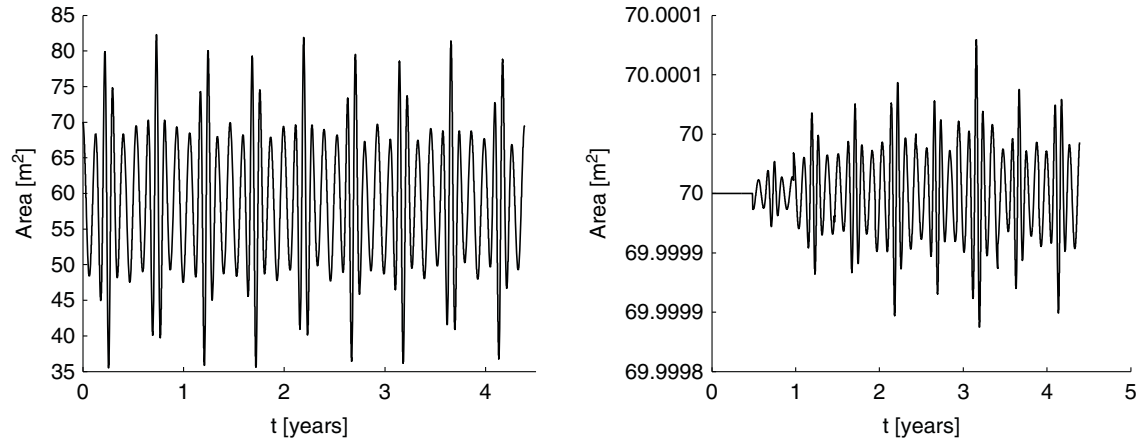

a) Area required: offset of −40 km in x axis

b) Area required: no offset in x axis

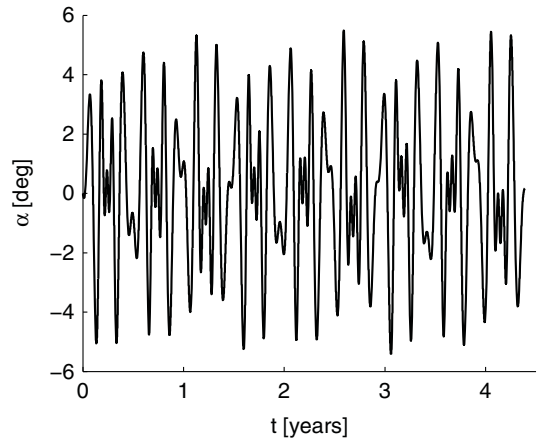

c) In-plane angle α: offset of −40 km in x axis

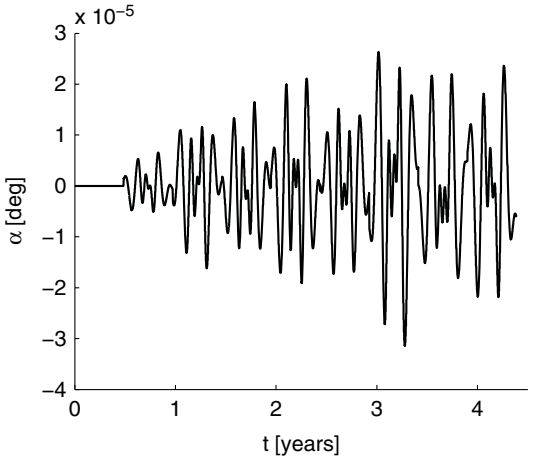

d) In-plane angle α: no offset in x axis

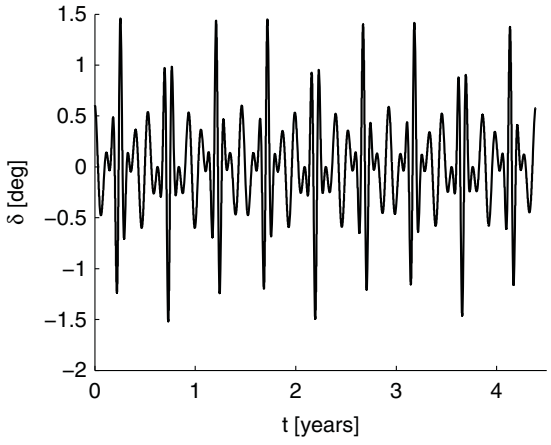

e) Out-of-plane angle δ: offset of −40 km in x axis

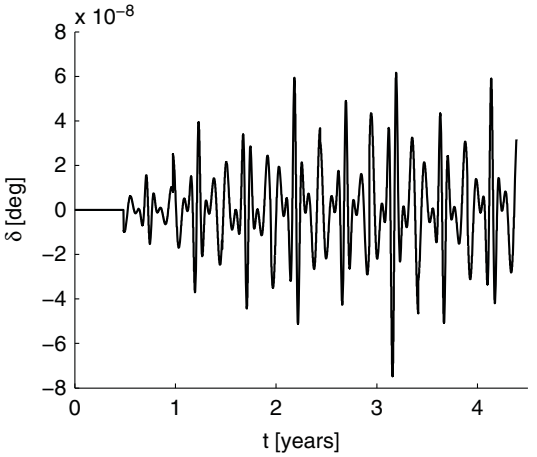

f) Out-of-plane angle δ: no offset in x axis

29 **Fig. 8 Comparison of the effect of the initial injection error along the x axis onto the reflective area and the orientation angle required for stabilizing the orbit when an initial area of 70 m^2 is selected.**

and conjugate eigenvalues occurs. The controller derived in Sec. III is used. The mass of the spacecraft is still 1000 kg and the gains required to stabilize the orbit are $G_1 = G_2 = G_3 = 31$. The controller is tested for the planar LPOs in Fig. 3a and for the DPO orbit shown in Fig. 3b. An initial reflective area of 4.5 m^2 is selected, and an initial offset along the x axis is included to avoid tiny control requirements. Figure 9 shows the required area and in-plane angle for the selected high-amplitude orbits. In this case, the controller cannot be pushed to a high injection error due to infeasible solutions; thus, minimum offsets of -1 and -0.5 km are selected for the LPO (Figs. 9a and 9c) and for the DPO (Figs. 9b and 9d), respectively. In both cases, a small offset required relatively high variations in area and in α if compared with the SOHO case study. This is because these orbits have an index of stability that is much smaller than halo orbits; thus, a small deviation from the target shows higher values in the control requirements. Therefore, high-amplitude orbits require a precise insertion maneuver with a tiny deviation from the target if the control is to be performed using SRP. However, the increase of the control gains may enlarge the effect of the control; thus, a small offset would not need high variations in area and α.

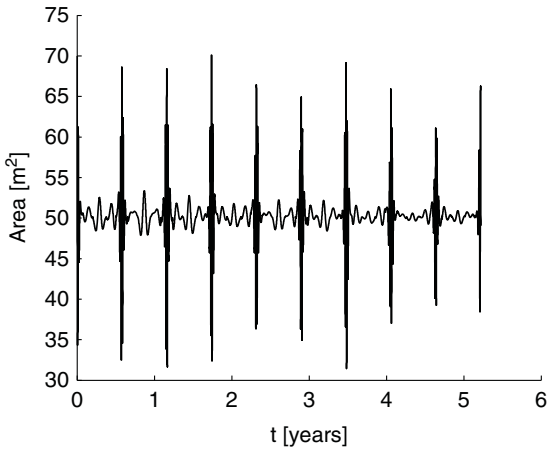

a)Area required for the planar LPO: offset of −1 km in *x* axis

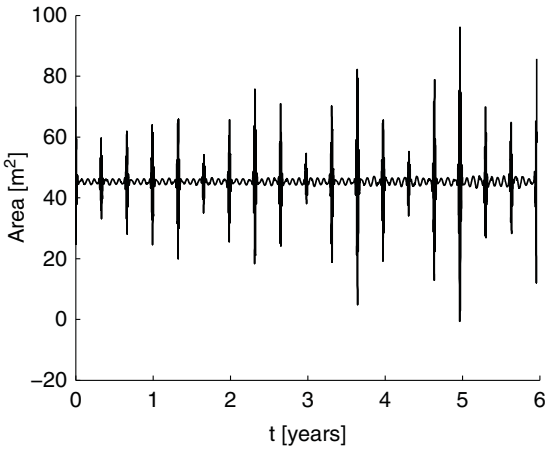

b) Area required for the DPO : offset of −0.5 km in *x* axis

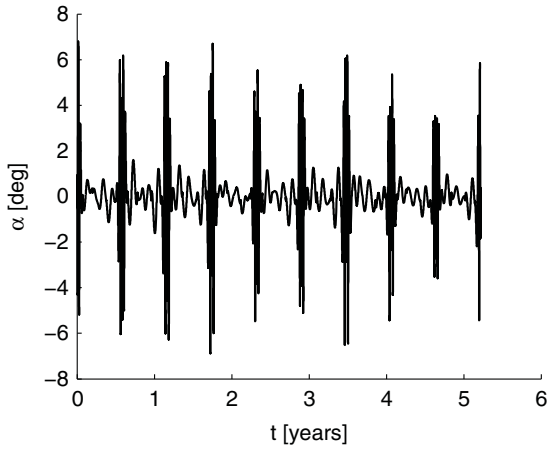

c) In-plane angle for the planar LPO α: offset of −1k min *x* axis

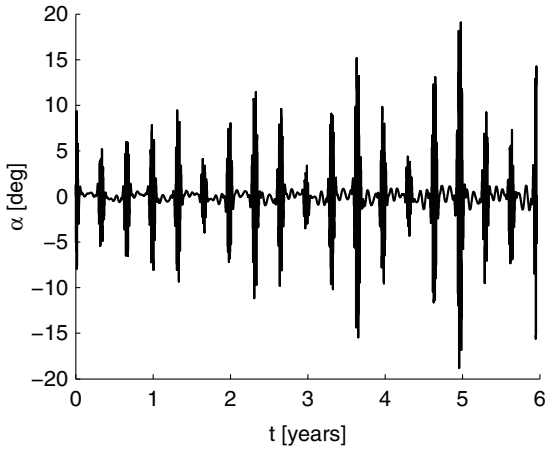

d) In-plane angle for the DPO α: offset of −0.5 km in *x* axis

Fig. 9 Area and in-plane angle required for the planar LPO in Fig. 3b and the DPO in Fig. 3a.

VIII. Deployable Structure Solutions

As shown in Sec. VII, the HSP control requires small variations in the reflective area and in the in-plane angle α. It is also found that the variation in the out-of plane angle δ is very small, on the order of $10^{-5} - 10^{-8}$ deg. Thus, in this case, the controller is effective in the variation of area and α. The variation in the angle α is achievable with the LPO's spacecraft pointing requirements. For example, the SOHO and Herschel spacecraft require a three-axis attitude stabilization with pointing accuracy of 1 arcsec; whereas the Gaia spacecraft is spin-axis stabilized, where the angle between the spin axis and the sun-line direction (shown in Fig. 10) is of 45 deg. The area variation of the reflective control actuators depends on the effect of the disturbances, where the initial offset of the spacecraft from the target orbit due to failure in the orbit insertion maneuver is evaluated.

In this section, the required additional flaps to achieve a variable-geometry actuator system are presented for a class of LPO spacecraft similar to the SOHO mission. Figure 10 shows an example of a nominal configuration[¶] for a spacecraft that has a near-perfect reflective deployable area of 20 m^2 and a mass of 1000 kg. The case studied is shown in Table 1 for $A_0 = 20$ m^2 when an initial offset in position of -5 km is considered. It is supposed that the square area of the spacecraft bus is not reflective (white prism in Fig. 10). The bus area is 11.61 m^2 (3.4073×3.4073 m). It is also assumed that one side of the solar array and of the reflective actuator flap match the side of the spacecraft bus with a width of 3.4073 m, as shown in Fig. 10. The SOHO spacecraft solar array is designed to have an area of 21.9 m^2. Each of the four solar paddles (darkest squares Fig. 10) thus has an area of 5.475 m^2. By knowing that the width of the solar paddle is 3.4073 m (as the solar bus size), the length of each of the four solar paddles is 1.6068 m.

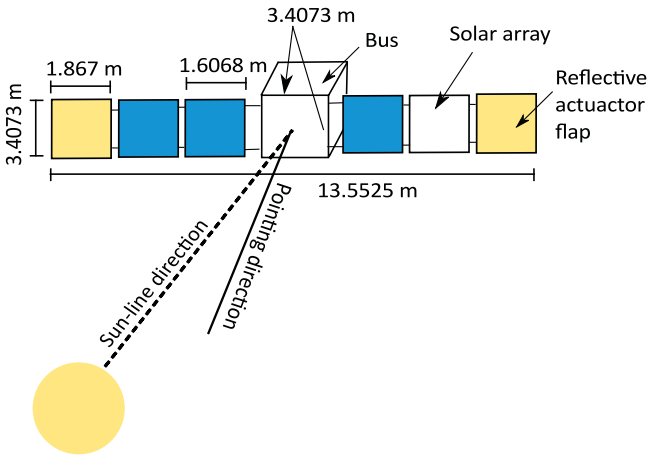

Fig. 10 Actuator configuration for a class of spacecraft like the SOHO mission.

From Table 1, the initial β_0 required for a near-perfect area is $3.06 \cdot 10^{-5}$. The reflectivity coefficient of the solar array C_r^{sa} is 1.08 at the beginning of life. The lightness parameter for the solar array β_{sa} can be calculated from Eq. (4).

[¶]The nominal configuration of the control area was previously denoted with A_0. It is the initial area before activating the control law.

The solar array lightness parameter β_{sa} for a 1000 kg spacecraft corresponds to $1.8227 \cdot 10^{-5}$. An initial near perfect reflective flap ($C_r^f = 2$) has to be added to reach the β_0 condition[**]. The lightness number associated to the nominal reflective flap β_0^f is given by the following:

$$\beta_0^f = \beta_0 - \beta_{\text{sa}} \tag{73}$$

The initial total area of the reflective flaps is 8.0867 m^2 ($\beta_0^f = 1.2373 \cdot 10^{-5}$). Two flaps of area $A_0^f = 4.0434$ m^2 (1.1867×3.4073 m) are required (lighter-colored boxes in Fig. 10).

Note that it is possible to sum the lightness numbers of different areas with different reflectivities because the definition of the equivalent reflectivity coefficient is given by the following:

$$C_r^* = \frac{2 \cdot C_r^f \cdot A_0^f + 4 \cdot C_r^{\text{sa}} \cdot A_{\text{sa}}}{2 \cdot A_0^f + 4 \cdot A_{\text{sa}}} \tag{74}$$

where C_r^* is an equivalent reflectivity coefficient. The total lightness number β_0 is given by Eq. (4), and it turns into

$$\begin{aligned} \beta_0 &= \frac{P^*}{m_{sc}}(2 \cdot A_0^f + 4 \cdot A_{sa}) \cdot C_r^* \\ &= \frac{P^*}{m_{sc}} \cdot (2 \cdot C_r^f \cdot A_0^f + 4 \cdot C_r^{\text{sa}} \cdot A_{\text{sa}}) = \beta_0^f + \beta_{\text{sa}} \end{aligned} \tag{75}$$

where m_{sc} is the total mass of the spacecraft and

$$P^* = P_{\text{srp-1AU}} \frac{r_{\text{Earth-Sun}}^2}{\mu_{\text{Sun}}}$$

From Eq. (75), it is clear that operations within lightness numbers of different reflective surfaces are possible.

The total length of the spacecraft in its nominal configuration is therefore 13.5525 m. The length of the SOHO spacecraft without the reflective actuator flaps was originally of 9.8 m.

As shown in Table 1 for a near-perfect reflective area[††] of $A_0 = 20$ m^2, the total area variation needed to meet the control requirements is between 15.5 and 21.5 m^2; thus, the variation in the total reflective area $2 \cdot \Delta A_0^f$ is to be between -4.5 and 1.5 m^2. For each reflective flap, the initial A_0^f has to be reduced by 2.25 m^2 (0.6603×3.4073 m) or increased by 0.75 m^2 (0.2201×3.4073 m). In summary, the minimum flap area is $A_{\text{min}}^f = 1.7934$ m^2 and the maximum flap area is $A_{\text{max}}^f = 4.7934$ m^2, whereas the nominal flap area is $A_0^f = 4.0434$ m^2.

The material proposed to design a highly reflective and light actuator flap uses solar sail technology. The best sail substrate is Kapton and has a surface density of 7.1 g/m^2. The best choice of the surface coating is aluminum with a surface density of 1.35 g/m^2 [31]. The maximum area of one flap is 4.7934 m^2, and the mass of the flap material is 40.5 g (0.0405 kg). To support the flap material, 7.9914 m of mast structure, as shown in Fig. 11, is required that has a linear mass of 70 g/m [40], which totals 560 g (0.56 kg). The total mass of one flap is therefore 600.5 g, and the total mass of the two flaps is 1.201 kg. Allowing a 20% mass margin [31], the total mass of the reflective actuator system is 1.4412 kg. Figure 11 shows the front and the back views of the reflective actuator flap with a maximum area of $A_{\text{max}}^f = 4.7934$ m^2.

Shahid and Kumar [17] proposed a sliding-mode control for LPO spacecraft enhanced by solar radiation pressure. In the Shahid and Kumar [17] case, the initial area required for the control was around 40 m^2. For a 1000 kg spacecraft, it was proposed by Shahid and Kumar [17] to use a solar sail with a final mass of 6 kg. In this work,

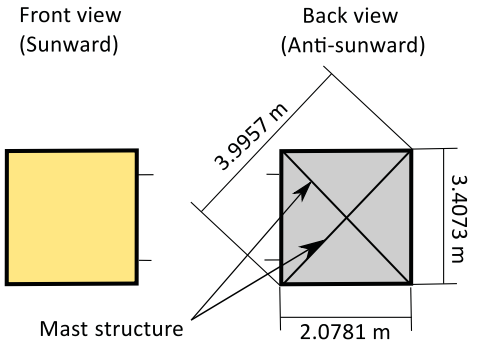

Fig. 11 Front and back views of the reflective actuator flap for $A_{\text{max}}^f = 4.7934$ m^2.

two additional flaps to the spacecraft solar array were proposed with a total area of 8.0867 m^2 and an additional mass of 1.4412 kg.

Table 2 summarizes the overall size of the spacecraft and the size in the reflective actuator flaps. Note that the nominal area is 20 m^2 for a near-perfect reflective area. However, the contribution of 21.9 m^2 of solar array was taken into account; thus, A_0 now includes the area of the near-perfect flaps and of the solar array with a reflectivity coefficient of 1.08. Due to the nonperfect reflective property of the solar array, a nominal area of 31.4868 m^2 is therefore required.

An example of variable-shape areas was proposed by Borggräfe et al. [41], who also suggested the use of electrochromic devices for the control of multipurpose variable-shape sails. Borggräfe et al. [41] considered distributed masses with variable reflectivity, allowing a change of the sail shape from a flat configuration (i.e., active trajectory control) to a parabolic shape for use as a remote sensing device or communication antenna. A similar approach can be adopted here by having a reflective actuator flap covered by the pixels of a reflective control device. The control law can thus be transformed in an electric impulse to switch on (highly reflective pixel; Fig. 12) and off (absorption pixel; Fig. 12) the reflective control devices. In this case, the shape of the flap is kept fixed and the effect of the variable geometry is obtained by changing the surface luminosity of the flaps. Figure 12 shows how to modify the reflective area of the flap through a reflective control device. The advantage of this method is in allowing the change of the reflective area without mechanical moving parts. This method could also add flexibility in the control law mission design. It would be possible to adjust the requirements of the control law by reshaping the on/off switching configuration. The main disadvantage is related to the effect of degradation of the material in the space environment; thus, a margin in the area should be included to compensate the effect of degradations during the duration of the mission.

Other options investigate the use of mechanism to change the geometry of the controlled area. Recently, Ceriotti et al. [42] proposed a variable-geometry cone sail, achieved using controlled mechanisms. Currently, mechanical solutions do not allow a continuous variation of the area; thus, the proposed controlled acceleration has to limit the fluctuation in the required area when using the current space mechanism. The continuous variable area requires the design of deployable mechanisms that enhance the variable shape of the SRP actuators. As previously stated, current space technology does not provide solutions for a continuously varying geometry actuator system. This suggests that further study

Table 2 Spacecraft area datasheet

Area	m^2	Number
Spacecraft bus	11.61	1
Solar paddle A_{sa}	5.475	4
Reflective actuator flap A_{max}^f	4.7934	2
Nominal area from Table 1 A_0	20	— —
Control area required from Table 1 $A_{\text{min}} - A_{\text{max}}$	15.5–21.5	— —
Nominal area needed; $A_0 = 4 \cdot A_{\text{sa}} + 2 \cdot A_0^f$	31.4868	— —
Variation of the reflective actuator $A_{\text{min}}^f - A_{\text{max}}^f$	1.7934–4.7934	2

**Note that $C_r^* = 2$ is a theoretical value, and it is true at the beginning of life; however, some concern should be given on the degradation of reflectivity due to the space environment.

††Note that, here, A_0 is the contribution of the solar array and the additional flaps area at the nominal condition; thus, $A_0 = 4 \cdot A_{\text{sa}} + 2 \cdot A_0^f$.

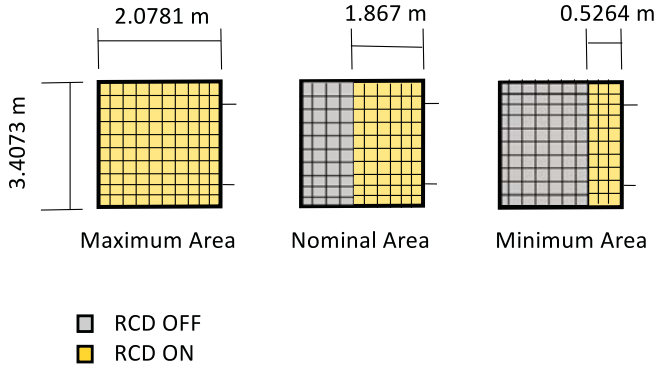

Fig. 12 Concept of pixel reflective control device.

should be done in the design of future space missions to find innovative solutions.

IX. Conclusions

This work focuses on the design of a solar radiation pressure Hamiltonian structure-preserving control for spacecraft. The Hamiltonian structure-preserving control law developed by Scheeres et al. [27] is here extended to high-amplitude orbits and applied by considering the effect of solar radiation pressure. The Hamiltonian structure-preserving control is a good candidate for solar radiation pressure applications because of the low control acceleration required (thus the fuel expenditure is small), the robustness due to error in the launcher orbit insertion maneuver, and how it works in the regime of nonlinearities. The Hamiltonian structure-preserving control stabilizes the orbit through the simple Lyapunov stability by counteracting the stable and unstable manifolds. Thus, the effect of the control is to add an artificial center manifold to the system. The Hamiltonian structure-preserving control is extended to high-amplitude orbits when couples of complex and conjugate eigenvalues occur. The generalized control shows that the control area pointing requirements match the LPO spacecraft pointing requirements where the major action of control is given in the in-plane angle rather than in the out-of-plane angle. This result holds independently from the orbit amplitude size. The most efficient control parameters are thus the reflective area and the in-plane angle α. A variable reflective area is required by the control law. In this paper, a pixel reflective control device (RCD) fixed-shape flap is proposed to enhance geometrical change in the area-to-mass ratio of the spacecraft without using a mechanism. This can provide a fast control response in the variation of the reflective area, and it can prevent demanding requirements to the AOCS subsystem. As high-amplitude orbits are highly unstable when compared with low-amplitude orbits, a spacecraft in high-amplitude orbits requires a precise orbit insertion maneuver and high reflective surfaces to keep the spacecraft on the nominal orbit.

Appendix A: Hamiltonian Structure-Preserving Control Law Extended to the Third Dimension

The eigenvalues of the linearized dynamics are the solutions of the characteristic equations $D(\lambda) = |Df - \lambda I| = 0$, where the characteristic polynomial is

$$\Lambda^3 + b\Lambda^2 + c\Lambda + d = 0 \tag{A1}$$

where b, c, and d are defined as follows:

$$\begin{cases} b = 4 - V_{xx} - V_{yy} - V_{zz} \\ c = -V_{xy}^2 - V_{xz}^2 + V_{xx}V_{yy} - V_{yz}^2 - 4V_{zz} + V_{xx}V_{zz} + V_{yy}V_{zz} \\ d = -|V_{rr}| \end{cases} \tag{A2}$$

The aim of the controller is to place the eigenvalues on the imaginary axis, so an artificial center manifold stabilizes the periodic orbit by removing the stable and unstable manifolds (i.e., hyperbolic equilibrium). The discriminant of the equation must be greater than zero in order to have three real and distinct roots:

$$\Delta = b^2c^2 - 4c^3 - 4b^3d - 27d^2 + 18bcd \tag{A3}$$

To have an instantaneous map of real eigenvalues and two pairs of imaginary eigenvalues, the polynomial in Eq. (A1) must have one positive and two negative roots. If $\Delta > 0$, there are three real and distinct solutions. For a cubic polynomial, it is possible to guarantee only one positive root by following the Descartes rule of signs. Thus, $b > 0$, $c < 0$, $d < 0$ (or $|V_{rr}| > 0$), and $\Delta > 0$. When $\Delta < 0$, there are two couples of complex and conjugate roots and one real root. However, the extension to this case is not included yet in our analysis.

1. Eigenvalues of the Characteristic Polynomial

The solutions of Eq. (A1) are [43] as follows:

$$Q = \frac{3c - b^2}{9}, \qquad R = \frac{9bc - 27d - 2b^3}{54},$$
$$S = (R + \sqrt{Q^3 + R^2})^{1/3}, \qquad T = (R - \sqrt{Q^3 + R^2})^{1/3} \tag{A4}$$

$$\begin{cases} \Lambda_1 = S + T - \dfrac{b}{3} \\ \Lambda_2 = -\dfrac{(S+T)}{2} - \dfrac{b}{3} + \dfrac{(S-T)\cdot i}{2} \\ \Lambda_3 = -\dfrac{(S+T)}{2} - \dfrac{b}{3} - \dfrac{(S-T)\cdot i}{2} \end{cases} \tag{A5}$$

So, now, we can find the six eigenvalues as $\lambda_1 = \sqrt{\Lambda_1}$, $\lambda_2 = -\sqrt{\Lambda_1}$, $\lambda_3 = \sqrt{\Lambda_2}$, $\lambda_4 = -\sqrt{\Lambda_2}$, $\lambda_5 = \sqrt{\Lambda_3}$, and $\lambda_6 = -\sqrt{\Lambda_3}$.

2. Eigenvectors of the Characteristic Polynomial

The eigenvectors can now be found by solving the system $(A - \lambda_i I) \cdot \hat{\boldsymbol{x}} = 0$:

$$\begin{cases} \dot{\hat{x}} = \lambda_i \hat{x} \\ \dot{\hat{y}} = \lambda_i \hat{y} \\ \dot{\hat{z}} = \lambda_i \hat{z} \\ (V_{xx} - \lambda_i^2)\hat{x} + (V_{xy} + 2\omega_0\lambda_i)\hat{y} + V_{xz}\hat{z} = 0 \\ (V_{xy} - 2\omega_0\lambda_i)\hat{x} + (V_{yy} - \lambda_i^2)\hat{y} + V_{yz}\hat{z} = 0 \\ V_{xz}\hat{x} + V_{yz}\hat{y} + (V_{zz} - \lambda_i^2)\hat{z} = 0 \end{cases} \tag{A6}$$

Setting an arbitrary parameter for $\hat{x} = 1$, one of the infinitive eigenvectors for λ_i can be determined. We are now interested in solving the following system:

$$\begin{cases} (V_{xx} - \lambda_i^2) + (V_{xy} + 2\omega_0\lambda_i)\hat{y} + V_{xz}\hat{z} = 0 \\ (V_{xy} - 2\omega_0\lambda_i) + (V_{yy} - \lambda_i^2)\hat{y} + V_{yz}\hat{z} = 0 \\ V_{xz} + V_{yz}\hat{y} + (V_{zz} - \lambda_i^2)\hat{z} = 0 \end{cases} \tag{A7}$$

which has three equations and two unknowns. Thus, we have three different options to find the solution. The general eigenvector is defined as follows:

$$\begin{Bmatrix} \hat{x} \\ \hat{y} \\ \hat{z} \\ \dot{\hat{x}} \\ \dot{\hat{y}} \\ \dot{\hat{z}} \end{Bmatrix} = \begin{Bmatrix} 1 \\ u_i \\ u_{2_i} \\ \lambda_i \\ \lambda_i \cdot u_i \\ \lambda_i \cdot u_{2_i} \end{Bmatrix} \tag{A8}$$

In the case of solving the first two equations of Eq. (A7), the solution is

$$\hat{y} = \frac{V_{xz}(V_{xy} - 2\omega_0\lambda_i) + V_{yz}(\lambda_i^2 - V_{xx})}{V_{yz}(V_{xy} + 2\omega_0\lambda_i) - V_{xz}(V_{yy} - \lambda_i^2)} = u_i$$
$$\hat{z} = \frac{(-V_{xy}^2 + 4\omega_0^2\lambda_i^2 - V_{yy}\lambda_i^2 + V_{yy}V_{xx} + \lambda_i^4 - \lambda_i^2 V_{xx})}{V_{yz}(V_{xy} + 2\omega_0\lambda_i) - V_{xz}(V_{yy} - \lambda_i^2)} = u_{2_i} \tag{A9}$$

If now we solve the first and the third equations of Eq. (A7), the solution becomes

$$\hat{y} = \frac{(V_{xx} - \lambda_i^2)(V_{zz} - \lambda_i^2) - V_{xz}^2}{V_{xz}V_{yz} - (V_{xy} + 2\omega_0\lambda_i)(V_{zz} - \lambda_i^2)} = u_i$$
$$\hat{z} = \frac{(V_{xy} + 2\omega_0\lambda_i)V_{xz} - (V_{xx} - \lambda_i^2)V_{yz}}{V_{xz}V_{yz} - (V_{xy} + 2\omega_0\lambda_i)(V_{zz} - \lambda_i^2)} = u_{2_i} \tag{A10}$$

Finally, by solving the second and third equations of Eq. (A7), the solution turns into

$$\hat{y} = \frac{(V_{xy} - 2\omega_0\lambda_i)(V_{zz} - \lambda_i^2) - V_{yz}V_{xz}}{V_{yz}^2 - (V_{yy} - \lambda_i^2)(V_{zz} - \lambda_i^2)} = u_i$$
$$\hat{z} = \frac{(V_{yy} - \lambda_i^2)V_{xz} - (V_{xy} - 2\omega_0\lambda_i)V_{yz}}{V_{yz}^2 - (V_{yy} - \lambda_i^2)(V_{zz} - \lambda_i^2)} = u_{2_i} \tag{A11}$$

Appendix B: Derivatives of the Solar Radiation Pressure Accelerations

In Sec. V, the control acceleration is given by the solar radiation pressure actuators, where knowledge of the Jacobian matrix in Eq. (68) is required. In this section, the derivatives of the SRP accelerations with respect to α (in-plane angle), δ (out-of-plane angle), and β (lightness parameter, function of the area-to-mass ratio) is shown. The spacecraft–sun vector is defined with respect to the rotating system by two angles: Φ (in-plane) and Ψ (out-of-plane). These two angles are functions of the spacecraft–sun vector components and are defined as follows:

$$\Phi = \arctan\left(\frac{y}{(x - x_{\text{Sun}})}\right), \quad \text{and} \quad \Psi = \arctan\left(\frac{z}{(x - x_{\text{Sun}})^2 + y^2}\right) \tag{B1}$$

respectively. The projection of the spacecraft–sun vector on the $x - y$ plane is defined as follows:

$$\boldsymbol{r}_{xy,\text{Sun}-p} = \sqrt{(x - x_{\text{Sun}})^2 + y^2} \tag{B2}$$

The partial derivatives of the SRP accelerations with respect to α are defined as follows:

$$\frac{\partial \boldsymbol{a}}{\partial \alpha} = \begin{Bmatrix} a_{x\alpha} \\ a_{y\alpha} \\ a_{z\alpha} \end{Bmatrix} \tag{B3}$$

where the components in x, y, and z are

$$a_{x\alpha} = \frac{\beta \cdot (\mu - 1)\cos(\delta + \Psi) \cdot [-2z \cdot \boldsymbol{r}_{xy,\text{Sun}-p}\cos(3\alpha/2 + \Phi)\sin(\alpha/2)\sin(\delta) + \cos(\delta)(z^2\sin(\alpha + \Phi) \cdot \boldsymbol{r}_{xy,\text{Sun}-p}^2\sin(2\alpha + \Phi))]}{[(x + \mu)^2 + y^2 + z^2]^{3/2}} \tag{B4}$$

$$a_{y\alpha} = \frac{-[\beta(\mu - 1)\cos(\delta + \Phi)(\cos(\delta)(z^2\cos(\alpha + \Psi) + \boldsymbol{r}_{xy,\text{Sun}-p}^2\cos(2\alpha + \Phi)) + 2z\boldsymbol{r}_{xy,\text{Sun}-p}\sin(\alpha/2)\sin(3\alpha/2 + \Psi))]}{[(x + \mu)^2 + y^2 + z^2]^{3/2}} \tag{B5}$$

and

$$a_{z\alpha} = \frac{\beta(\mu - 1)\sin(\alpha)[\boldsymbol{r}_{xy,\text{Sun}-p}^2\cos(\delta) - z\boldsymbol{r}_{xy,\text{Sun}-p}\sin(\delta)\sin(\delta + \Psi)]}{[(x + \mu)^2 + y^2 + z^2]^{3/2}} \tag{B6}$$

As for the partial derivatives in α, the definition for the derivatives in δ is

$$\frac{\partial \boldsymbol{a}}{\partial \delta} = \begin{Bmatrix} a_{x\delta} \\ a_{y\delta} \\ a_{z\delta} \end{Bmatrix} \tag{B7}$$

where the partial derivative in x is

$$a_{x\delta} = \frac{\beta(1 - \mu)\cos(\alpha + \Psi)[\cos(\delta + \Phi)(-z\boldsymbol{r}_{xy,\text{Sun}-p}(-1\cos(\alpha))\cos(\delta) - (z^2 + \boldsymbol{r}_{xy,\text{Sun}-p}^2\cos(\alpha))\sin(\delta))}{[(x + \mu)^2 + y^2 + z^2]^{3/2}}$$
$$- \frac{((z^2 + \boldsymbol{r}_{xy,\text{Sun}-p}^2\cos(\alpha))\cos(\delta) - z\boldsymbol{r}_{xy,\text{Sun}-p}(-1\cos(\alpha))\sin(\delta))\sin(\delta + \Phi)]}{[(x + \mu)^2 + y^2 + z^2]^{3/2}} \tag{B8}$$

the derivative in y is

$$a_{y\delta} = \frac{\beta(1 - \mu)\sin(\alpha + \Phi)[\cos(\delta + \Psi)(-z\boldsymbol{r}_{xy,\text{Sun}-p}(-1\cos(\alpha))\cos(\delta) - (z^2 + \boldsymbol{r}_{xy,\text{Sun}-p}^2\cos(\alpha))\sin(\delta))}{[(x + \mu)^2 + y^2 + z^2]^{3/2}}$$
$$- \frac{((z^2 + \boldsymbol{r}_{xy,\text{Sun}-p}^2\cos(\alpha))\cos(\delta) - z\boldsymbol{r}_{xy,\text{Sun}-p}(-1 + \cos(\alpha))\sin(\delta))\sin(\delta + \Psi)]}{[(x + \mu)^2 + y^2 + z^2]^{3/2}} \tag{B9}$$

whereas the derivative in z is

$$a_{z\delta} = \frac{\beta(1-\mu)[\cos(\delta+\Psi)((z^2+\boldsymbol{r}^2_{xy,\mathrm{Sun}-p}\cos(\alpha))\cos(\delta) - z\boldsymbol{r}_{xy,\mathrm{Sun}-p}(-1\cos(\alpha))\sin(\delta))}{[(x+\mu)^2+y^2+z^2]^{3/2}} \\ \frac{(-z\boldsymbol{r}_{xy,\mathrm{Sun}-p}(-1\cos(\alpha))\cos(\delta) - (z^2\boldsymbol{r}^2_{xy,\mathrm{Sun}-p}\cos(\alpha))\sin(\delta))\sin(\delta+\Psi)]}{[(x+\mu)^2+y^2+z^2]^{3/2}} \tag{B10}$$

For the case of the derivatives in β, the solution is written in a compact way as follows:

$$\frac{\partial \boldsymbol{a}}{\partial \beta} = (1-\mu)\left\langle \frac{\boldsymbol{r}_{\mathrm{Sun}-p}}{|+_{\mathrm{Sun}-p}|}, \hat{N}\right\rangle^2 \cdot \hat{N} \tag{B11}$$

In Eq. (B11), the scalar product between the spacecraft–sun vector and the normal vector to the reflective surface is defined by

$$\left\langle \frac{\boldsymbol{r}_{\mathrm{Sun}-p}}{|\boldsymbol{r}_{\mathrm{Sun}-p}|}, \hat{N}\right\rangle \\ = \frac{(z^2+(y^2+(x+\mu)^2)\cos(\alpha))\cos(\delta) - z\cdot\boldsymbol{r}_{xy,\mathrm{Sun}-p}(\cos(\alpha)-1)\sin(\alpha)}{(x+\mu)^2+y^2+z^2} \tag{B12}$$

where the normalized spacecraft–sun vector is a function, by definition, of the angles Φ and Ψ:

$$\frac{\boldsymbol{r}_{\mathrm{Sun}-p}}{|\boldsymbol{r}_{\mathrm{Sun}-p}|} = \begin{Bmatrix} \cos(\Phi)\cdot\cos(\Psi) \\ \sin(\Phi)\cdot\cos(\Psi) \\ \sin(\Psi) \end{Bmatrix} \tag{B13}$$

Acknowledgments

Part of this work was funded by EPSRC DTP/CDT through grant 12 EP/K503150/1. S. Soldini would like to thank the anonymous reviewers for their valuable insights and detailed comments on how this journal in its original form could be improved.

References

[1] Szebehely, V., *Theory of Orbits in the Restricted Problem of Three Bodies*, Academic Press, New York, 1967, Chaps. 1, 7.

[2] Gordon, S. C., "Orbit Determination Error Analysis and Comparison of Station-Keeping Costs for Lissajousw and Halo-Type Libration Point Orbits and Sensitivity Analysis Using Experimental Design Techniques," NASA Rept. N93-24721, Feb. 1993, pp. 395–409.

[3] Perozzi, E., and Ferraz-Mello, S., *Space Manifold Dynamics: Novel Spaceways for Science and Exploration*, Springer, New York, 2010, Chaps. 1, 7. doi:10.1007/978-1-4419-0348-8

[4] Farquhar, R. W., "Halo-Orbit and Lunar-Swingby Missions of the 1990's," *Acta Astronautica*, Vol. 24, 1991, pp. 227–234. doi:10.1016/0094-5765(91)90170-A

[5] Olive, J. P., Overbeek, T. V., and Fleck, B., "SOHO Monthly Trending Report," Rept. SOHO/PRG/TR/769, 2013.

[6] Bauske, R., "Operational Manoeuvre Optimization for the ESA Missions Herschel and Planck," *Proceedings of the 21st International Symposium on Space Flight Dynamics (ISSFD)*, Toulouse, France, Sept. 2009.

[7] Hechler, M., and Cobos, J., "Herschel, Planck and Gaia Orbit Design," *Proceedings of the 7th International Conference on Libration Point Orbits and Application*, Parador d'Aiguablava, Girona, Spain, June 2002.

[8] Canalias, E., Gómez, G., Marcote, M., and Masdemont, J. J., "Assessment of Mission Design Including Utilization of Libration Points and Weak Stability Boundaries," Ariadna id: 03/4103, 2004.

[9] Hénon, M., "Numerical Exploration of the Restricted Problem. V," *Astronomy and Astrophysics*, Vol. 1, 1968, pp. 223–238.

[10] Franz, H., , D'Amario, L. A., and Sackett, L. L.et al., "Wind Lunar Backflip and Distant Prograde Orbit Implementation," *Proceedings of the AAS/AIAA Spaceflight Mechanics*, Vol. 108, 2001, pp. 999–1017.

[11] Lara, M., and Russell, R., "Concerning the Family g of the Restricted Three-Body Problem," *Proceedings of the IX Jornadas de Trabajo en Mecanica Celeste*, Jaca, Hesca, Spain, 2006.

[12] Farrés, A., Jorba, Á., Mondelo, J. M., and Villac, B., "Periodic Motion for an Imperfect Solar Sail Near an Asteroid," *Proceedings of the 3rd International Symposium on Solar Sailing*, Glasgow, Scotland, U.K., June 2013.

[13] Scheeres, D. J., *Orbital Motion in Strongly Perturbed Environments*, Springer, New York, 2012, p. 350, Chap. 18.

[14] Noam, T., Karen, R., David, F., and Kimberly, T., "Using Solar Radiation Pressure to Control L_2 Orbits," *Proceedings of the AAS/GFC International Symposium on Space Flight Dynamics*, Vol. 100, May 1998, pp. 617–627.

[15] Sohon, R. L., "Attitude Stabilization by Means of Solar Radiation Pressure," *ARS Journal*, Vol. 29, 1995, pp. 371–373. doi:10.1016/0038-092X(59)90167-7

[16] Xin, M., Balakrishnan, S. N., and Pernicka, H. J., "Libration Point Stationkeeping Using the θ-D Technique," *Journal of the Astronautical Sciences*, Vol. 56, No. 2, 2008, pp. 231–250. doi:10.1007/BF03256550

[17] Shahid, K., and Kumar, K. D., "Spacecraft Formation Control at the Sun-Earth L_2 Libration Point Using Solar Radiation Pressure," *Journal of Spacecraft and Rockets*, Vol. 47, No. 4, 2010, pp. 614–626. doi:10.2514/1.47342

[18] Gómez, G., Llibre, J., Matinez, R., Simó, C., and Rodriguez, J., "On the Optimal Station Keeping Control of Halo Orbits," *Acta Astronautica*, Vol. 15, No. 6, 1987, pp. 391–397. doi:10.1016/0094-5765(87)90175-5

[19] Gómez, G., Llibre, J., Matínez, R., and Simó, C., *Dynamics and Mission Design Near Libration Points — Volume I: Fundamentals: The Case of Collinear Libration Points*, Vol. 2, World Scientific Monograph Series in Mathematics, World Scientific, Singapore, ROS, 2001.

[20] Howell, K. C., and Pernicka, H. J., "Stationkeeping Method for Libration Point Trajectories," *Journal of Guidance, Control, and Dynamics*, Vol. 16, No. 1, 1993, pp. 151–159. doi:10.2514/3.11440

[21] Keeter, M., "Station-Keeping Strategies for Libration Point Orbits: Target Points and Floquét Mode Approaches," M.S. Thesis, Purdue Univ., West Lafayette, IN, 1994.

[22] McInnes, A. I. S., "Strategies for Solar Sail Mission Design in the Circular Restricted Three-Body Problem," M.S. Thesis, Purdue Univ., West Lafayette, IN, 2000.

[23] Farrés, A., and Jorba, Á., "A Dynamical System Approach for the Station Keeping of a Solar Sail," *Journal of the Astronautical Sciences*, Vol. 56, No. 2, 2008, pp. 199–230. doi:10.1007/BF03256549

[24] Farrés, A., and Jorba, Á., "Dynamics of a Solar Sail Near a Halo Orbit," *Acta Astronautica*, Vol. 67, Nos. 7–8, 2010, pp. 979–990. doi:10.1016/j.actaastro.2010.05.022

[25] Ceriotti, M., and Farrés, A., "Solar Sail Station Keeping of High-Amplitude Vertical Lyapunov Orbits in the Sun-Earth System," *Proceedings of the 63rd International Astronautical Congress*, Naples, Italy, Oct. 2012.

[26] Farrés, A., and Jorba, Á., "Station Keeping of a Solar Sail Around a Halo Orbit," *Acta Astronautica*, Vol. 94, No. 1, 2014, pp. 527–539. doi:10.1016/j.actaastro.2012.07.002

[27] Scheeres, D. J., Hsiao, F. Y., and Vinh, N. X., "Stabilizing Motion Relative to an Unstable Orbit: Applications to Spacecraft Formation Flight," *Journal of Guidance, Control, and Dynamics*, Vol. 26, No. 1, Jan. 2003, pp. 62–73. doi:10.2514/2.5015

[28] Xu, M., and Xu, S., "Structure-Preserving Stabilization for Hamiltonian System and its Applications in Solar Sail," *Journal of Guidance, Control, and Dynamics*, Vol. 32, No. 3, May 2009, pp. 997–1004. doi:10.2514/1.34757

[29] Bookless, J., and McInnes, C., "Control of Lagrange Point Orbits Using Solar Sail Propulsion," *Acta Astronautica*, Vol. 62, Nos. 2–3, 2008,

pp. 159–176.
doi:10.1016/j.actaastro.2006.12.051

[30] Koon, W. S., Lo, M. W., Marsden, J. E., and Ross, S. D., *Dynamical Systems, The Three-Body Problem and Space Mission Design*, Marsden Books, 2008, Chaps. 2, 23.

[31] McInnes, C. R., *Solar Sailing: Technology, Dynamics and Mission Applications*, Springer, Glasgow, Scotland, U.K., 1998, Chaps. 2, 32.

[32] Biggs, J. D., McInnes, C., and Waters, T., "New Periodic Orbits in the Solar Sail Restricted Three Body Problem," *Proceedings of the 2nd Conference on Nonlinear Science and Complexity*, Porto, Portugal, 2008.

[33] Vallado, D. A., *Foundamentals of Astrodynamics*, Space Technology Library, 2004.

[34] Khalil, H., *Nonlinear Systems*, Prentice–Hall, Upper Saddle River, NJ, 2002, Chaps. 4, 111.

[35] Ginoux, J.-M., *Differential Geometry Applied to Dynamical Systems*, Nonlinear Science, Vol. 66, 2009, Chaps. 3, 41.

[36] Kuchment, P., *Floquet Theory for Partial Differential Equations*, Vol. 60, Operator Theory: Advances and Applications, Switzerland, 1993.

[37] Xu, M., and Zhu, J., "Applications of Hamiltonian Structure-Preserving Control to Formation Flying on a J2-Perturbed Mean Circular Orbit," *Celestial Mechanics and Dynamical Astronomy*, Vol. 113, No. 4, 2012, pp. 403–433.
doi:10.1007/s10569-012-9430-2

[38] Xu, M., and Liang, Y., "Cluster Flight Control for Fractionated Spacecraft on an Elliptic Orbit," *Celestial Mechanics and Dynamical Astronomy*, Vol. 125, No. 4, 2016, pp. 383–412.
doi:10.1007/s10569-016-9685-0

[39] Tsuda, Y., Mori, O., Funase, R., Sawada, H., Yamamoto, T., Saiki, T., Endo, T., Yonekura, K., Hoshino, H., and Kawaguchi, J., "Achievement of IKAROS—Japanese Deep Space Solar Sail Demonstration Mission," *Acta Astronautica*, Vol. 82, No. 2, 2013, pp. 183–188.
doi:10.1016/j.actaastro.2012.03.032

[40] Murphy, D., and Macy, B., "Demonstration of a 10 m Solar Sail System," *45th AIAA/ASME/ASCE/AHS/ASC Structures, Structural Dynamics and Material Conference*, AIAA Paper 2004-1576, 2004, pp. 698–708.

[41] Borggräfe, A., Heiligers, J., Ceriotti, M., and McInnes, C. R., "Distributed Reflectivity Solar Sail for Extended Mission Applications," *3rd International Symposium on Solar Sailing 2012 (ISSS 2013)*, 2013.

[42] Ceriotti, M., Harkness, P., and McRobb, M., "Variable-Geometry Solar Sailing: The Possibility of the Quasi-Rhombic Pyramid," *Proceedings of the 3rd International Symposium on Solar Sailing*, Glasgow, Scotland, U.K., 2013.

[43] Spigel, M. R., Lipschutz, S., and Liu, J., *Schaum's Outline of Mathematical Handbook of Formulas and Tables*, McGraw–Hill, New York, 2013, Chaps. V, 116.

Queries

1. AU: Please check that the copyright (©) type is correct. Please note that the code will be added upon publication.
2. AU: As AIAA only allows job titles in the affiliation footnotes, please note that degrees have been removed.
3. AU: Definitions of acronyms and abbreviations were moved from the abstract into the text of the article, per AIAA style.
4. AU: As AIAA only displays vectors in bold, and without arrows over them, please check that all variables are displayed correctly.
5. AU: Please clarify/define “Earth+moon”.
6. AU: The sentence beginning “In particular, L1 is located...” is unclear/incomplete. Please review and edit as necessary.
7. AU: Major syntax adjustments were made throughout the paper for clarity; please read closely to confirm that your meaning was retained.
8. AU: Please define ISEE-3, CSA, and SOHO.
9. AU: Please clarify the meaning of “instead” in the sentence beginning “Distant prograde orbits (DPOs) are,...”.
10. AU: Please define OTS, TELECOM 1, and INMARSAT 2.
11. AU: Please define FM.
12. AU: Please define AU.
13. AU: Some of the sentences were edited to begin with capital letters, per journal guidelines. Please confirm your meaning was retained.
14. AU: Please clarify the use of “instead” in the sentence beginning “Instead, α and δ are the angles...”.
15. AU: Instructions from AIAA indicate that figures are to appear in color only online. Please verify the usage of color in your proof is correct, and note that all figures will be grayscale in the print journal.
16. AU: Please note that some of the inline equations were made into display equations for readability and per journal guidelines.
17. AU: Please provide the appropriate citation/reference for “Scheeres demonstrated”.
18. AU: Please provide the appropriate citation/reference for “As exploited by Scheeres”.
19. AU: As the figures will only appear in color online, and the text will be the same both online and in print, references to color have been removed and/or edited throughout. Please confirm your meaning was retained.
20. AU: AIAA prefers that figure captions be 3–12 words long. The captions to Figs. 3 and 8 far exceed this limit. Please reduce the lengths of these captions to no more than 12 words and/or incorporate the information into the text.
21. AU: Citations have been added throughout the paper, per journal guidelines. Please confirm they are correct.

22. AU: Please review and edit "by placing the eigenvalues of the linearized dynamics, the eigenvalues, on the imaginary axis, as shown in Fig. 4, by adding to V_{rr} an artificial potential, the center manifold T" for clarity.

23. AU: Please review and edit the sentence beginning "If we now focus on the short-term..." for clarity.

24. AU: Please note that, if quotation marks are used to set off an unusual term in the text, AIAA requires them to be deleted from subsequent usage of the same term.

25. AU: Please note that AIAA requires acronyms be used more than once to remain in the paper.

26. AU: JAXA was defined as Japan Aerospace Exploration Agency. Please confirm this is correct.

27. AU: Please define IKAROS.

28. AU: Please confirm the term "hyberbolic" is correct.

29. AU: Please confirm the y-axis values of Fig. 8b are correct.

30. AU: Please define EPSRC DTP/CDT.

31. AU: Please provide the issue numbers and/or months of publication for Refs. [4, 9, 15].

32. AU: For Ref. [3], please provide the name and location of the institution.

33. AU: If Refs. [6, 7, 11, 12, 25, 32, 41, 42] are published proceedings, please provide the names and locations of the publishers (NOT of the conference hosts) and the page ranges. If they are conference papers, please provide the paper numbers and the organizers' names.

34. AU: For Ref. [8], please provide additional information to help the reader find the reference (e.g., journal title, volume, issue, and page range; book title, publisher name and location, and pages used; or institution name and location with report number).

35. AU: For Ref. [10], please provide the names of all of the authors, as well as the name and location of the publisher (NOT the conference host).

36. AU: For Ref. [14], please provide the full name and location of the publisher (NOT the conference host).

37. AU: Please provide the pages used for Ref. [19].

38. AU: For Refs. [33, 36], please provide the names and locations of the publishers, as well as the pages sued.

39. AU: For Refs [30, 35], please provide the locations of the publishers.

40. AU: References appearing only in the appendices were relabelled, per journal guidelines. Please check that all citations are correct.